Optimal Driving for Vehicle Fuel Economy under Traffic Speed Uncertainty

Fuliang Wu[a], Tolga Bektaş[*,b], Ming Dong[a], Hongbo Ye[c], and Dali Zhang[d]

[a] *Antai College of Economics and Management, Shanghai Jiao Tong University, Shanghai 200030, China. E-mail:* `wfl_sjtu@sjtu.edu.cn` *(Wu),* `mdong@sjtu.edu.cn` *(Dong)*
[b] *University of Liverpool Management School, University of Liverpool, Liverpool L69 7ZH, UK. E-mail:* `T.Bektas@liverpool.ac.uk`
[c] *School of Engineering, University of Liverpool, Liverpool L69 3GH, UK. E-mail:* `Hongbo.Ye@liverpool.ac.uk`
[d] *Sino-US Global Logistics Institute, Antai College of Economics and Management, Shanghai Jiao Tong University, Shanghai 200030, China, E-mail:* `zhangdl@sjtu.edu.cn`

Abstract

Minimizing the amount of fuel consumed by a moving vehicle can be formulated as an optimal control problem that determines the speed profile that the vehicle should follow. The fuel consumption is generally a function of speed and acceleration, and is optimized under external parameters (e.g., road grade or surrounding traffic conditions) known to affect fuel economy. Uncertainty in the traffic conditions, and in particular traffic speed, has seldom been investigated in this context, which may prevent the vehicle from following the optimal speed profile and consequently affect the fuel economy and the journey time. This paper describes two stochastic optimal speed control models for minimizing the fuel consumption of a vehicle traveling over a given stretch of road under a given time limit, where the maximum speed that can be achieved by the vehicle over the journey is assumed to be random and follow a certain probability distribution. The models include chance constraints that either (i) limit the probability that the desired vehicle speed exceeds the traffic speed, or (ii) bound the probability that the journey time limit is violated. The models are then extended into distributionally robust formulations to capture any uncertainties in the probability distribution of the traffic speed. Computational results are presented on the performance of the proposed models and to numerically assess the impact of traffic speed variability and journey duration on the desired speed trajectories: The results affirm that uncertainty in traffic speeds can significantly increase the amount of fuel consumption and the journey time of the speed profiles created by deterministic model. Such increase in journey duration can be mitigated by incorporating the stochasticity at the planning stage using the models described in this paper, and more so with the distributionally robust formulations particularly with higher levels of uncertainty. The solutions themselves generally exhibit low levels of speeds, which ensure the feasibility of the speed profile against any variabilities in the traffic speed.

Keywords: optimal control; fuel consumption; uncertain traffic speed; stochastic programming; distributional robustness

*Corresponding author.

1 Introduction

Vehicle fuel consumption is significantly affected by the style of driving. Minimizing the amount of fuel consumed by a vehicle traveling on a given road, sometimes within a limited time period and assuming a terminal speed, is usually referred to as *eco-driving, trajectory optimization* or *speed optimization*, and can be formulated as an optimal control problem. Trajectory optimization problems have been studied in both online and offline applications. The online application is solved en-route, and determines the optimal speed and control strategies under actual traffic conditions as the vehicle travels. In contrast, the offline application determines the optimal speed profile that the vehicle should follow before the journey takes place, and is relevant to the planning problems where the decisions are often taken the 'day-before' and cannot be easily changed once made (Bektaş et al., 2019).

The most relevant work on trajectory optimization can be traced back to Schwarzkopf and Leipnik (1977), who were probably the first to develop an optimal control model of motor vehicle throttle settings to minimize fuel consumption under varying road conditions. With the increasing amount of research on this topic, particularly due to the emergence of autonomous vehicles, most studies require the availability of complete information on the traffic conditions when planning the vehicle speeds, and assume that the vehicle will be able to drive at their desired speeds as planned. Limited attention however has been given to a more practical situation where uncertain traffic conditions, due to the factors such as weather-related events or traffic congestion, may limit the maximum achievable speeds of the vehicle and render the planned speeds infeasible. Ignoring the uncertainty at the planning stage may yield suboptimal solutions and result in higher fuel consumption (Nasri et al., 2018).

Incorporating such uncertainties in the optimal speed control problem can help to ensure that the planned speed profile is robust against variations in maximum achievable speeds, which is the motivation and the aim of this paper. In particular, the problem we study here is to determine the speed profile (trajectory) of a vehicle traveling from an origin to a destination under a prescribed time limit so as to minimize the amount of fuel consumed. We describe two stochastic optimal speed control models, where the maximum achievable speeds dictated by the exogenous traffic conditions are modeled as probabilistic variables. The first formulation enforces that the planned speeds should be achievable with a certain probability. The second formulation ensures that the vehicle arrives at the destination in the given time limit with a certain probability. Our proposed methods are extensions of the eco-driving problem by considering the uncertain traffic speed to minimize fuel consumption through optimizing the speed profile. The methods proposed here are designed for use at the planning stage, i.e., before the trip commences, and prescribe the speed profile before the vehicle starts the journey and before the actual traffic speeds are known.

The rest of our paper is organized as follows. Section 2 briefly reviews the related literature on optimal speed control problems. Section 3 introduces the deterministic optimal speed control model and the solution methods. The two stochastic optimal speed control models are described in Section 4, which are then extended into distributionally robust formulations in Section 5. Case study and numerical experiments are presented in Section 6. The paper concludes in Section 7.

2 Literature review

In this section, we first present a detailed review on the deterministic optimal speed control problem relevant to vehicle energy minimization, followed by a brief overview of the relevant literature on the optimal speed control problem incorporating urban driving conditions such as behavior of other vehicles.

2.1 The deterministic optimal speed control problem

The deterministic optimal speed control problem optimizes the instantaneous (e.g., second-by-second) speed and acceleration of a vehicle traveling along a given stretch of road to minimize the amount of energy or fuel consumed. It is an application of optimal control on highways, where all data relevant to the journey, such as destination and altitude, are assumed to be known beforehand. The two main types of solution methods are analytical and numerical.

Schwarzkop and Leipnik (1977) formulated the optimal speed control problem using a nonlinear fuel consumption model, and derived closed-form analytical solutions for constant road slopes using Pontryagin's maximum principle (Kopp, 1962). The results suggested that it is possible to optimize fuel consumption on a level road using a constant speed. Chang and Morlok (2005) used methods of calculus to show that the optimal speed trajectory is a constant speed and numerically confirmed the theoretical results. Fröberg et al. (2006) studied optimal speed profiles for heavy-goods trucks, and found that constant speed is optimal for minimizing fuel consumption on level roads and those with a small gradient. Passenberg et al. (2009) developed a hybrid optimal control model for operating trucks, where the objective function comprises economical income and fuel consumption, derived optimality conditions analytically and evaluated them numerically. Ozatay et al. (2014) linearized the longitudinal vehicle dynamics around the optimal constant speed, approximated the fuel consumption with a simplified nonlinear model, and described an analytical method to solve the optimal control problem.

Dynamic Programming (DP) is a more general technique that has been used to solve the optimal speed control problem for a range of fuel consumption models and can yield speed profiles for different road conditions. DP solves a discretized version of the problem using an iterative process. Hooker et al. (1983) described a DP to solve the optimal speed control problem that incorporates time- and location-dependent constraints such as speed limits and trip time. Later, Hooker (1988) applied the method to a variety of vehicles, and calculated the optimal speed trajectories over different roads. Monastyrsky and Golownykh (1993) relaxed the trip duration constraint by incorporating it into the objective function, through which they calculated the speed trajectories indirectly by adjusting the weights on fuel consumption and trip duration. By doing so, the running time of the DP was significantly reduced. Hellström et al. (2006, 2009) formulated the optimal speed control problem as being dependent on the vehicle position rather than time, so that the road gradient can be easily incorporated into the model. Using the same technique, location-dependent speed limits can also be modeled (Maamria et al., 2016a). Hellström et al. (2010) showed that using kinetic energy as the independent variable in the model formulation can avoid oscillating solutions and reduce linear interpolation errors. Luján et al. (2018) investigated the potential reduction in fuel consumption and NO_x emissions by optimizing the speed trajectory. Liu et al. (2020) integrated the vehicle routing problem with the optimal speed control problem by considering the load-dependent vehicle dynamics, and developed a simultaneous routing-and-control algorithm to solve it. The application of their algorithm on several case studies yielded better solutions with respect to fuel consumption and time when compared to a sequential approach.

Whilst the publications reviewed above predominantly concern conventional vehicles, similar energy optimal control models have been described in other contexts such as electric vehicles (EVs), hybrid-electric vehicles (HEVs), and trains.

Compared to conventional vehicles, EVs behave differently as regards energy consumption, leading to different control and state variables, and objective functions (Lim et al., 2016). In particular, a unique feature of an EV is the regenerative braking system, which provides negative torque to the drive wheels and converts kinetic energy into electricity to recharge the battery (Xu et al., 2011). Petit and Sciarretta (2011) studied eco-driving for an EV with a DC-type motor, where the electric power demanded by the electric machine was represented using an analytical expression. Dib et al. (2014) investigate optimal energy management in eco-driving for an EV that is assumed to be powered by a permanent-magnet synchronous machine, and the vehicle trajectory itself is constrained by the infrastructure and other vehicles. For an eco-driving optimal control problem, Maamria et al. (2016b) used a battery model represented by an equivalent circuit model comprising voltage source and electric resistance, both of which are related to the state-of-charge of the battery.

The powertrain of an HEV is more complex due to the two sources of energy for the internal combustion engine and the electric motor. Consequently, improving the fuel efficiency of an HEV relies on the control strategy used for the energy sources (Heppeler et al., 2014). Energy management for hybrid vehicles has been studied by Sciarretta and Guzzella (2007), Pisu and Rizzoni (2007) and Bender et al. (2013). Combining eco-driving and hybrid powertrains can lead to further efficiencies in fuel economy. Kim et al. (2009) proposed a model predictive controller to optimize both the speed profile and the torque split. van Keulen et al. (2010) estimated the speed trajectory and the corresponding power trajectory to optimize the power split trajectory between the two energy sources via Energy Management Systems (EMS). Mensing et al. (2012) used the battery state-of-charge in identifying the energy optimal speed trajectory. Later, Heppeler et al. (2014) used DP to jointly optimize torque split, gear shift and speed trajectory. More recently, Guo et al. (2016) proposed an energy management strategy using model predictive control for HEVs, and proposed a bi-level methodology to reduce the computational time required to optimize the control variables.

Optimal speed control has also been extensively studied for trains. In addition to analytical methods based on Pontryagain's maximum principle (e.g., Albrecht et al., 2016 a & b), other numerical methods, including dynamic programming (Franke et al., 2000), nonlinear programming (Wang et al., 2013; Ye and Liu, 2016, 2017), and mixed integer linear programming (MILP) (Wang et al., 2011, 2013), were also widely applied to solve the problem. Wang et al. (2011, 2013) proposed a method that uses MILP and showed that it is able to solve the optimal speed trajectory problem faster than some DP and nonlinear programming methods.

2.2 Uncertainty in optimal driving

Vehicles running on open roads are often subject to a wide range of traffic conditions, such as those due to the infrastructure (e.g., road signs and signals) (De Nunzio et al., 2016; Wu et al., 2015; Yang et al. 2016) or other vehicles. Recent work on speed optimization problems has considered traffic signals and vehicle platoons (Gong and Du, 2018; Han et al., 2018; Ma et al., 2017; Ojeda et al., 2017; Zhao et al., 2018; Zhou et al., 2017), generally assuming that any information on movement of other vehicles in a platoon is deterministic and fully known at the time of planning. Such an assumption may not always hold in real driving conditions, because the behavior of drivers in traffic can be uncertain or even unpredictable. The exclusion of such uncertainties in determining the speed profiles may yield suboptimal or even infeasible trajectories in practice.

More relevant to our paper is the uncertainty in attainable speeds due to the uncertain behavior of other drivers, which can limit the maximum speed of an ego vehicle (i.e., the vehicle that is being controlled). For example, when the ego vehicle is moving in a single lane following another vehicle, the ego vehicle should always maintain a safety distance to the predicting vehicle, and any decision made on the speed of the ego vehicle should consider the possible changes in the speed of the preceding vehicle (Wei et al., 2011). There has been a broad range of research activity on trajectory optimization, particularly for autonomous vehicles, that considers the uncertain movements of surrounding vehicles, for which we refer the readers to the comprehensive reviews by Katrakazas et al. (2015) and Claussmann et al. (2019). To the best of our knowledge, all such methods require real time traffic information in the area surrounding the vehicle. Our models break away from this body of work; in particular we are concerned with pre-trip speed planning where the ego vehicle does not need to know the actual traffic speeds.

2.3 Contribution

As mentioned above, to the best of our knowledge, the approaches described in the existing body of research reviewed above are reactive in that they can deal with uncertainties that reveal themselves in real time as the ego vehicle travels. There is, therefore, still a need for approaches that are able to proactively determine the speed trajectory of a vehicle when the uncertainties in traffic conditions are expected to affect the vehicle speed. This is particularly relevant to operational- or tactical-level planning problems that involve the choice of optimal speed (Bektaş and Laporte, 2011).

Our study aims to address this aspect and contributes to the existing body of research in three ways. *First*, we represent the uncertainty of traffic speeds in the optimal speed control problem in the form of upper bounds on the maximum achievable speeds that are modeled by probabilistic parameters. We describe two stochastic optimal speed optimization models that impose bounds on the probability that the planned speeds or the maximum allowable journey duration is violated, and further extended these formulations to cater for distributional robustness. *Second*, we present methods to reformulate the optimal control models and linearize their discretized formulations so that the proposed optimization problems can be solved using off-the-shelf optimization software. *Third*, we perform extensive computational analyses under different scenarios, to numerically evaluate the performance of the proposed models and to assess the impact of traffic speed variability and journey duration on the desired speed trajectories.

3 Deterministic optimal speed control model

In this section, we present the classical optimal speed control model that assumes deterministic input parameters and use discretization to recast the problem as a nonlinear program (NLP) and subsequently as a mixed integer program (MIP). The techniques described in this section form the basis of the subsequent formulations for the stochastic optimal speed control problem that will be presented in Section 4.

3.1 Problem description

The deterministic optimal control problem concerns finding the optimal speed trajectory for a vehicle on a straight road, starting from an origin at time 0, destined to a location at S units distance, and is required to arrive at the destination within T units of time. For the problem to be feasible, T should be larger than the amount of time required to traverse the road where the vehicle runs at the upper speed limits allowed by road conditions and traffic.

We denote distance s from the origin node as the independent variable, and the nonzero vehicle speed $v(s)$ and acceleration $a(s)$ at distance s as the state and control variables, respectively. The aim is to minimize the total fuel consumed by the vehicle over the journey, calculated using an instantaneous fuel consumption function $FR(v(t), a(t))$. A formulation for the problem is given as follows (Hooker et al., 1983; Monastyrsky and Golownykh, 1993; Luján et al., 2018):

$$\underset{a(s)}{\text{Minimize}} \quad \int_0^S FR(v(s), a(s)) \frac{1}{v(s)} \mathrm{d}s \tag{3.1}$$

subject to

$$\int_0^S \frac{1}{v(s)} \mathrm{d}s \leq T \tag{3.2}$$

$$a(s) = \frac{\mathrm{d}v(s)}{\mathrm{d}s} v(s) = \frac{\mathrm{d}v(s)^2}{2\mathrm{d}s} \qquad s \in [0, S] \tag{3.3}$$

$$a_{\min} \leq a(s) \leq a_{\max} \qquad s \in [0, S] \tag{3.4}$$

$$\epsilon \leq v(s) \leq v_{\max}(s) \qquad s \in [0, S] \tag{3.5}$$

$$v(0) = v_0, v(S) = v_S, \tag{3.6}$$

where $a_{\min}$ is the minimum acceleration or maximum deceleration, which can be negative,

$a_{\max}$ is the constant maximum acceleration dictated by the maximum engine power, ϵ is a sufficiently small positive value, $v_{\max}(s)$ is the maximum speed at which the vehicle is allowed to travel at distance s from the origin, and v_0 and v_S are the initial and terminal speeds, respectively.

The objective (3.1) is to minimize the fuel consumption over the whole journey. Constraint (3.2) enforces the vehicle to arrive at the terminal location within time T. Constraint (3.3) describes the relationship between speed and acceleration. Constraints (3.4)–(3.5) set the lower and upper bounds for acceleration and speed, respectively. Constraints (3.6) set the fixed initial speed and terminal speed, respectively. Note that the terminal speed constraint is optional (Hooker,1988).

3.2 Solution methods

In this section, we use discretization to recast the optimal speed control model as a NLP formulation, which is then reformulated as a MIP formulation subject to linear constraints that allows the use of off-the-shelf software to solve the problem.

3.2.1 Discretization-based nonlinear programming

Discretization is a standard method to solve the optimal control formulation of the eco-driving problems (Hooker et al., 1983; Monastyrsky and Golownykh, 1993; Hellström et al., 2009). It operates on the basis of dividing the total length S of the road into n segments of uniform length $\Delta s = S/n$. The fuel consumed in traversing each segment is calculated based on the initial speed and the acceleration on the segment, where the acceleration is assumed to be constant over each segment. The fuel consumed over the entire journey is equal to the sum of fuel consumed over all segments.

With a little abuse of notation, let $0, 1, ..., n-1$ represent the segment indices, where segment k corresponds to the segment of distance $[(k-1)\Delta s, k\Delta s]$ from the origin. For each segment $k \in \{0, 1, ..., n-1\}$, let $\theta(k)$ be the average road slope, $a(k)$ be the constant acceleration, and $v(k)$ and $v_{\max}(k)$ be the desired speed and maximum allowable speed at the beginning of the segment, respectively. The optimal speed control model (3.1)–(3.6) is then discretized as the following NLP:

$$\underset{a(k)}{\text{Minimize}} \quad \sum_{k=0}^{n-1} FR(v(k), a(k)) \frac{\Delta s}{v(k)} \tag{3.7}$$

subject to

$$\sum_{k=0}^{n-1} \frac{\Delta s}{v(k)} \le T \tag{3.8}$$

$$a(k) = \frac{v(k+1)^2 - v(k)^2}{2\Delta s} \qquad k \in \{0, 1, ..., n-1\} \tag{3.9}$$

$$a_{\min} \le a(k) \le a_{\max} \qquad k \in \{0, 1, ..., n-1\} \tag{3.10}$$

$$\epsilon \le v(k) \le v_{\max}(k) \qquad k \in \{1, ..., n-1\} \tag{3.11}$$

$$v(0) = v_0, v(n) = v_S, \tag{3.12}$$

where $v(n)$ represents the speed at the end of segment $n-1$, which is the destination. Note that constraints (3.9)–(3.10) are nonconvex. In the following subsection, we will reformulate (3.7)–(3.12) into a mixed integer program with linear constraints, so as to solve the model more efficiently.

3.2.2 Mixed integer programming

We follow the technique and definition introduced by Wang et al. (2013). First, we define a new decision variable $E(k) = \frac{1}{2}v(k)^2$ representing the kinetic energy per unit mass at the beginning of each $k \in \{0, 1, ..., n-1\}$. Then the nonlinear model (3.7)–(3.12) can be reformulated as follows:

$$\underset{a(k)}{\text{Minimize}} \quad \sum_{k=0}^{n-1} FR(\sqrt{2E(k)}, a(k)) \frac{\Delta s}{\sqrt{2E(k)}} \tag{3.13}$$

subject to

$$\sum_{k=0}^{n-1} \frac{\Delta s}{\sqrt{2E(k)}} \le T \tag{3.14}$$

$$a(k) = \frac{E(k+1) - E(k)}{\Delta s} \qquad k \in \{0, 1, ..., n-1\} \tag{3.15}$$

$$a_{\min} \le a(k) \le a_{\max} \qquad k \in \{0, 1, ..., n-1\} \tag{3.16}$$

$$\frac{1}{2}\epsilon^2 \le E(k) \le \frac{1}{2}v_{\max}(k)^2 \qquad k \in \{1, ..., n-1\} \tag{3.17}$$

$$E(0) = \frac{1}{2}v_0^2, \ E(n) = \frac{1}{2}v_S^2, \tag{3.18}$$

The above model is still nonlinear due to the term $\frac{1}{\sqrt{2E(k)}}$ in the objective function and constraint (3.15). Following Wang et al. (2013), we approximate $f(E(k)) = \frac{1}{\sqrt{2E(k)}}$ using a piecewise affine (PWA) function. For the purposes of illustration, we present such a PWA function with three linear pieces, given by the following equation and illustrated in

Figure 1,

$$f_{\mathrm{PWA}}(E(k)) = \begin{cases} \lambda_1 E(k) + \gamma_1, & \text{for} \quad E_{\min} \leq E(k) \leq E_1 \\ \lambda_2 E(k) + \gamma_2, & \text{for} \quad E_1 < E(k) \leq E_2 \\ \lambda_3 E(k) + \gamma_3, & \text{for} \quad E_2 < E(k) \leq E_{\max}, \end{cases} \tag{3.19}$$

where λ_1, λ_2, λ_3 and γ_1, γ_2, γ_3 are the slopes and intercepts of the linear functions, respectively, $E_{\min} = \frac{1}{2}\epsilon^2$, $E_{\max} = \max\{\frac{1}{2}v_{\max}(k)^2 \ , \forall k \in \{0, 1, 2, ..., n-1\}\}$, and E_1 and E_2 are the intersections of the adjacent pieces of the PWA function. Note that the values of these parameters are the same for all k. Increasing the number of linear pieces in the PWA function can improve the accuracy of the approximation, which will be tested later in our computational experiments in Section 6.

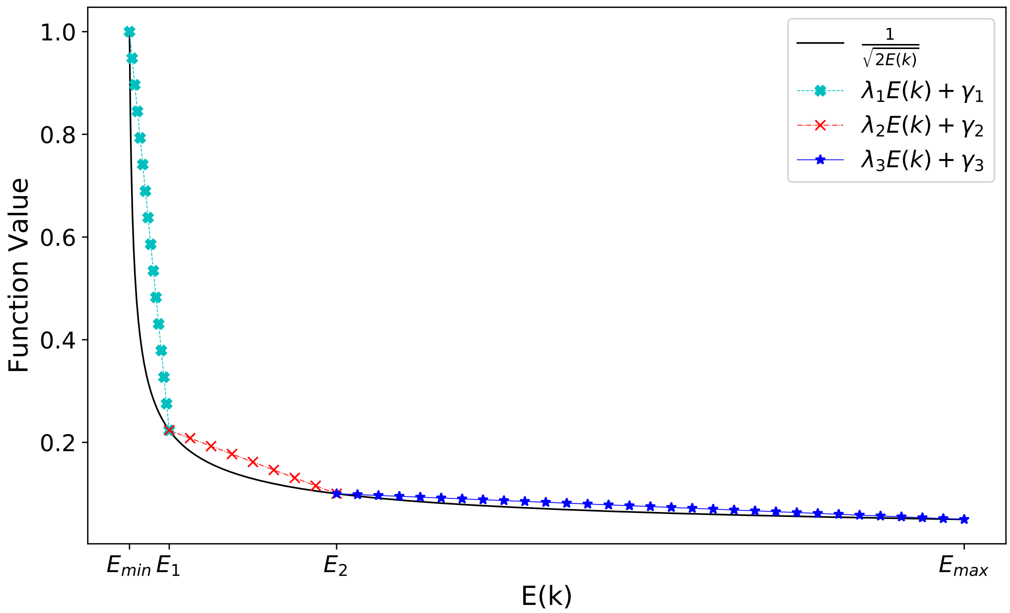

Figure 1: The PWA function

In order to incorporate the piecewise linear functions into the formulation, we introduce two new binary variables, namely $\delta_1(k)$ that is equal to 1 if $E(k) \leq E_1$, and to 0 otherwise, and $\delta_2(k)$ that is equal to 1 if $E(k) \leq E_2$, and to 0 otherwise. Then, expression (3.19) can be formulated as follows,

$$\begin{aligned} f_{\mathrm{PWA}}(E(k)) = {} & \delta_1(k)\delta_2(k)(\lambda_1 E(k) + \gamma_1) + (1 - \delta_1(k))\delta_2(k)(\lambda_2 E(k) + \gamma_2) \\ & + (1 - \delta_1(k))(1 - \delta_2(k))(\lambda_3 E(k) + \gamma_3) \end{aligned} \tag{3.20}$$

subject to

$$E(k) \leq (E_{\max} - E_1)(1 - \delta_1(k)) + E_1 \tag{3.21}$$
$$E(k) \geq E_1 + \varepsilon + (E_{\min} - E_1 - \varepsilon)\delta_1(k) \tag{3.22}$$
$$E(k) \leq (E_{\max} - E_2)(1 - \delta_2(k)) + E_2 \tag{3.23}$$
$$E(k) \geq E_2 + \varepsilon + (E_{\min} - E_2 - \varepsilon)\delta_2(k), \tag{3.24}$$

where ε is a sufficiently small constant due to the "strictly less" conditions in Eq. (3.19). To linearize the product $\delta_1(k)\delta_2(k)$ in (3.20), we introduce a third binary variable $\delta_3(k)$ to replace $\delta_1(k)\delta_2(k)$, along with the following set of constraints:

$$-\delta_1(k) + \delta_3(k) \leq 0 \tag{3.25}$$
$$-\delta_2(k) + \delta_3(k) \leq 0 \tag{3.26}$$
$$\delta_1(k) + \delta_2(k) - \delta_3(k) \leq 1. \tag{3.27}$$

Finally, we define new auxiliary variables $z_1(k) = \delta_1(k)E(k)$, $z_2(k) = \delta_2(k)E(k)$, and $z_3(k) = \delta_3(k)E(k)$ to replace the nonlinear term in (3.20), subject to the following set of linear inequalities:

$$z_j(k) \leq E_{\max}\delta_j(k) \qquad j \in \{1,2,3\} \tag{3.28}$$
$$z_j(k) \geq E_{\min}\delta_j(k) \qquad j \in \{1,2,3\} \tag{3.29}$$
$$z_j(k) \leq E(k) - E_{\min}(1 - \delta_j(k)) \quad j \in \{1,2,3\} \tag{3.30}$$
$$z_j(k) \geq E(k) - E_{\max}(1 - \delta_j(k)) \quad j \in \{1,2,3\}. \tag{3.31}$$

Substituting $z_1(k)$, $z_2(k)$, $z_3(k)$ and $\delta_3 = \delta_1\delta_2$ into the piecewise function (3.20) yields the following linear expression:

$$\begin{aligned} f_{\text{PWA}}(E(k)) \;=\; & -\lambda_3 z_1(k) + (\lambda_2 - \lambda_3)z_2(k) + (\lambda_1 - \lambda_2 + \lambda_3)z_3(k) \\ & -\gamma_3\delta_1(k) + (\gamma_2 - \gamma_3)\delta_2(k) + (\gamma_1 - \gamma_2 + \gamma_3)\delta_3(k) \\ & +\lambda_3 E(k) + \gamma_3. \end{aligned} \tag{3.32}$$

Subject to constraints (3.21)–(3.31), where $\delta_1, \delta_2, \delta_3$ are binary variables. By incorporating the reformulation (3.32) and the associated constraints above into the NLP formulation (3.13)–(3.18), we can obtain the following MIP formulation:

$$\underset{a(k)}{\text{Minimize}} \quad \sum_{k=0}^{n-1} FR(\sqrt{2E(k)}, a(k))\frac{\Delta s}{\sqrt{2E(k)}}\Delta s \tag{3.33}$$

subject to

$$\sum_{k=0}^{n-1} \Delta s f_{\text{PWA}}(E(k)) \leq T \tag{3.34}$$

$$(3.15)\text{–}(3.18),\ (3.21)\text{–}(3.32).$$

At this point, we observe that the constraints of the MIP above are all linear, and the nonlinear objective function (3.33) in the MIP above can be linearized if the fuel consumption model follows a particular structure. This is, for example, the case with the widely-used comprehensive modal emissions model (CMEM) shown below:

$$FR(v,a) = C_1 + C_2 \max\{Ma + \frac{1}{2}C_d\rho A v^2 + MgC_r\cos\theta + Mg\sin\theta, 0\}v, \tag{3.35}$$

where its formulation and the parameters are explained in detail in Appendix A. With the CMEM model, the objective (3.33) reads,

$$\begin{aligned} \underset{a(k)}{\text{Minimize}} \quad & \sum_{k=0}^{n-1} \left\{C_1 + C_2 X(k)\sqrt{2E(k)}\right\} \frac{\Delta s}{\sqrt{2E(k)}} \\ & = \sum_{k=0}^{n-1} \left\{C_1 f_{PWA}(E(k)) + C_2 X(k)\right\} \Delta s, \end{aligned} \tag{3.36}$$

subject to the following constraints:

$$X(k) \geq Ma(k) + C_d\rho A E(k) + Mg\sin\theta(k) + C_r Mg\cos\theta(k) \quad k \in \{0,1,...,n\} \tag{3.37}$$

$$X(k) \geq 0 \quad k \in \{0,1,...,n-1\}, \tag{3.38}$$

where $X(k)$ is introduced to linearize the term $\max\{\cdot, 0\}$ in (3.35). This finally results in a MILP consisting of (3.15)–(3.18), (3.21)–(3.32), (3.34) and (3.36)–(3.38), which can be solved by off-the-shelf optimization packages.

4 Stochastic optimal speed control

The optimal control models described in the preceding section set deterministic bounds on the speeds that can be chosen along a journey. In practice, however, the maximum achievable speeds on a road segment depend on the traffic conditions, which could be a result of the behaviour of the preceding vehicle(s) that the ego vehicle may need to follow throughout the journey, and thus are not always known with certainty prior to commencing the journey. The maximum speed $v_{\max}(s)$ at distance s from the origin will therefore have to obey the traffic speed, which is a random variable and can be correlated with the traffic speeds at other locations. We assume that the maximum speeds over the whole journey follow a multivariate distribution P. A few previous studies have investigated the real traffic data and suggested various distributions for the vehicle speeds on road, such as normal (Leong, 1968), skew-normal (Zou and Zhang, 2011), and composite distributions (Park et al., 2010). In general, the unimodal curve provides a good fit for the speed distribution under homogenous traffic conditions, but the distribution of speeds becomes more complex when the traffic conditions are heterogeneous (Park et al., 2010). In our models, we do not assume any particular distribution for P. Here we differentiate between the *planned (desired) speeds* $v(s)$ that are the output of an optimal control model at which the vehicle is planned to be driven, and the *actual (realized) speeds* at which the vehicle is actually driven, and potentially constrained by traffic speeds $v_{\max}(s)$. In particular, when the vehicle is en-route, if $v(s) \geq v_{\max}(s)$, then the actual (realized) speed will be equal to $v_{\max}(s)$.

In this section, we describe two stochastic optimal speed control models to incorporate the uncertainty in the traffic speed. The first model uses a chance constraint to ensure that the planned speeds can be achieved with a certain probability. The second model also uses chance constraints, but impose a bound on the probability of completing the journey within the prescribed time T. The latter is particularly relevant, as any uncertainty in traffic speeds along the journey is likely to impact the achievable speeds, and therefore the journey duration.

4.1 Chance constraints on the vehicle speed

The stochastic model presented in this section is similar to the deterministic optimal speed control model described in Section 3.1, with the difference being that the speed limit $v_{\max}(s)$ is now a random variable representing the uncertainty in the traffic speed. The following chance constraint (4.1) is used in place of (3.5),

$$\begin{aligned} \text{Prob}\left\{v(s) \leq v_{\max}(s)\right\} \geq \quad & 1-\alpha \qquad \forall s \in [0, S] \qquad (4.1)\\ v(s) \geq \quad & \epsilon \qquad \forall s \in [0, S], \qquad (4.2)\end{aligned}$$

which enforces that the desired speeds along the journey are achievable with probability $1-\alpha$. Then, the stochastic optimal speed control model with speed chance constraints is given by (3.1)–(3.4), (3.6), (4.1)–(4.2), which we will refer to as StoVer1.

The stochastic optimal speed control model can be reformulated as an approximate discretized stochastic nonlinear programming model in the same way as was done for the deterministic optimal speed control model described in Section 3.2.1. In particular, let $v_{\max}(k)$ be the traffic speed over segment $k = 0, 1, ..., n-1$, which follows a marginal distribution P_k based on the distribution P . Then, the chance constraint (4.1) can be replaced by the following inequalities:

$$\text{Prob}\left\{v(k) \le v_{\max}(k)\right\} \ge 1-\alpha \quad k \in \{1, ..., n-1\}. \tag{4.3}$$

Using the unit-mass kinetic energy $E(k) = \frac{1}{2}v(k)^2$ for each segment k as the decision variable, the chance constraint (4.3) above is equivalent to

$$\begin{aligned} & \text{Prob}\left\{v(k) \le v_{\max}(k)\right\} \ge 1-\alpha, \quad k \in \{1, 2, ..., n-1\} \\ \iff \quad & \text{Prob}\left\{2E(k) \le v_{\max}(k)^2\right\} \ge 1-\alpha, \quad k \in \{1, 2, ..., n-1\}, \end{aligned} \tag{4.4}$$

where the underlying probability distribution for the parameter $v_{\max}^2$ can be easily computed by using the distribution P of the traffic speed $v_{\max}$.

4.2 Chance constraints on the journey duration

In this subsection, we model the condition that the vehicle should arrive at the terminal location within the given time period T with a certain probability. In particular, the stochastic optimal speed control model that we present below includes a chance constraint stating that the probability of the duration being greater than T is at most α. In what follows, we first present the model in its original form, followed by a NLP formulation that uses discretization, and then a reformulation of the NLP as a MIP.

4.2.1 Stochastic optimal speed control model

As mentioned before, at a distance s from the origin, if the desired vehicle speed $v(s)$ is higher than the maximum allowable speed $v_{\max}(s)$, then the latter will be the *actual speed* to be implemented. The actual speed on the journey can therefore be expressed as $\min\{v(s), v_{\max}(s)\}$. The nonlinearity of this expression introduces further complications in the modeling, which we resolve as in the below.

We first introduce a new variable $a_r(s)$ to denote the actual acceleration at distance s, which can be used for calculating the fuel consumption. Similar to (3.3), the actual acceleration is calculated from the actual speed as follows:

$$a_r(s) = \frac{\mathrm{d}\min\{v(s), v_{\max}(s)\}}{\mathrm{d}s} \min\{v(s), v_{\max}(s)\}, \tag{4.5}$$

In principle, we should require the actual acceleration to be achievable, i.e., to be bounded by the maximum deceleration and maximum acceleration as the following constraints:

$$a_{\min} \le a_r(s) \le a_{\max}. \tag{4.6}$$

which is satisfied if the traffic acceleration and planned acceleration are both bounded. In practice, the traffic acceleration is bounded as specified by the following Assumption.

Assumption 4.1. *Let $a_t(s)$ denote the rate of change in the actual traffic speed $v_{\max}(s)$. Then,*

$$a_{\min} \leq a_t(s) = \frac{\mathrm{d}v_{\max}(s)}{\mathrm{d}s} v_{\max}(s) \leq a_{\max}, \tag{4.7}$$

for all $s \in [0, S]$. In other words, the traffic speed is bounded by the maximum deceleration and maximum acceleration.

Remark 4.1. *The practical interpretation of Assumption 4.1 is that the traffic speed is assumed not to change too quickly. This is reasonable since the acceleration and deceleration of each vehicle in the traffic is bounded due to their powering and braking capacities.*

If Assumption 4.1 holds, the planned acceleration is also bounded, i.e., $a_{\min} \leq a(s) = \frac{\mathrm{d}v(s)}{\mathrm{d}s} v(s) \leq a_{\max}$, then the actual acceleration will also be bounded by $a_{\min}$ and $a_{\max}$, which means that constraint (4.6) is satisfied.

The stochastic optimal control model is then formulated below:

$$\underset{a(s)}{\text{Minimize}} \quad \mathbb{E}_P \int_0^S FR\Big(\min\{v(s), v_{\max}(s)\}, a_r(s)\Big) \frac{1}{\min\{v(s), v_{\max}(s)\}} \mathrm{d}s \tag{4.8}$$

subject to

$$a_r(s) = \frac{\mathrm{d}\min\{v(s), v_{\max}(s)\}}{\mathrm{d}s} \min\{v(s), v_{\max}(s)\} \qquad s \in [0, S] \tag{4.9}$$

$$\text{Prob}\left\{\int_0^S \frac{1}{\min\{v(s), v_{\max}(s)\}} \mathrm{d}s \leq T\right\} \geq 1 - \alpha \tag{4.10}$$

$$a(s) = \frac{\mathrm{d}v(s)}{\mathrm{d}s} v(s) \qquad s \in [0, S] \tag{4.11}$$

$$a_{\min} \leq \ a(s) \ \leq \ a_{\max} \qquad s \in [0, S] \tag{4.12}$$

$$v(s) \geq \epsilon \qquad s \in [0, S] \tag{4.13}$$

$$v(0) = v_0, \ v(S) = v_S. \tag{4.14}$$

The objective (4.8) minimizes the expected fuel consumption over the journey. Constraint (4.9) computes the actual acceleration of the vehicle. The inequality (4.10) is the chance constraint that bounds the probability of the vehicle arriving at the terminal location within time T to be at least $1 - \alpha$. Constraint (4.12) bounds the change rate of the desired speed, and therefore limits the actual acceleration as explained earlier.

The main difficulty in solving the optimal control model above is due to the chance constraint (4.10), which requires integration over all random variables on the whole journey. To address this difficulty, we first present the following proposition.

Proposition 4.1. *Let $\nu : [a,b] \to \mathbb{R}^+$, and $\varphi : [a,b] \to \mathbb{R}$ be two functions. Define the set $\Omega = \left\{ \varphi \middle| \int_a^b \mathrm{d}\varphi(x) = z \right\}$, where z is a prespecified constant. Then, the following two sets I and J are equivalent:*

1. $I = \left\{ \nu \;\middle|\; \int_a^b \frac{1}{\nu(x)} \mathrm{d}x \le z \right\}$;
2. $J = \bigcup_{\varphi \in \Omega} \left\{ \nu \;\middle|\; \frac{1}{\nu(x)} \le \frac{\mathrm{d}\varphi(x)}{\mathrm{d}x} \ \forall x \in [a,b] \right\}$.

Proof. For any $x \in [a,b]$, we prove for both sufficiency and necessity.

1. $I \Rightarrow J$. For a $\nu \in I$, let $c = z - \int_a^b \frac{1}{\nu(x)} \mathrm{d}x \ge 0$. Define $\varphi(x) = \int_a^x \left(\frac{1}{\nu(x)} + \frac{c}{b-a} \right) \mathrm{d}x$, then $\mathrm{d}\varphi(x) = \left(\frac{1}{\nu(x)} + \frac{c}{b-a} \right) \mathrm{d}x$, then $\int_a^b \mathrm{d}\varphi(x) = \int_a^b \left(\frac{1}{\nu(x)} + \frac{c}{b-a} \right) \mathrm{d}x = z$ and $\frac{\mathrm{d}\varphi(x)}{\mathrm{d}x} = \frac{1}{\nu(x)} + \frac{c}{b-a} \ge \frac{1}{\nu(x)}$. So $\varphi \in \Omega$ and thus $\nu \in J$.

2. $J \Rightarrow I$. For a $\nu \in J$, there must exist a $\varphi \in \Omega$ such that $\frac{1}{\nu(x)} \le \frac{\mathrm{d}\varphi(x)}{\mathrm{d}x}$ for all $x \in [a,b]$. Then, $\int_a^b \frac{1}{\nu(x)} \mathrm{d}x \le \int_a^b \mathrm{d}\varphi(x) = z$, implying $\nu \in I$.

Combining 1 and 2 completes the proof. ■

Proposition 4.1 allows reformulating the chance constraint (4.10) in to the constraints (4.15)–(4.16) as follows:

$$\int_0^S \mathrm{d}t^*(s) = T \tag{4.15}$$

$$\mathrm{Prob}\left\{ \frac{1}{\min\{v(s), v_{\max}(s)\}} \le \frac{\mathrm{d}t^*(s)}{\mathrm{d}s}, \ \forall s \in [0,S] \right\} \ge 1 - \alpha. \tag{4.16}$$

In (4.15)–(4.16), $t^*(s)$ is a new variable that we call the *boundary time*, which can be interpreted as an upper bound to the point in time that the vehicle reaches distance s from the origin. Constraint (4.16) is a joint chance constraint of all the traffic speeds along the journey, which introduces further complexities as compared to an individual chance constraint (Chen et al. 2010). To overcome this issue, we relax the constraint as in the following proposition. We will later show in the numerical case studies in Section 6.2 that such a relaxation works well.

Proposition 4.2. *The following constraint (4.17) is a relaxation of constraint (4.16),*

$$\mathrm{Prob}\left\{ \frac{1}{\min\{v(s), v_{\max}(s)\}} \le \frac{\mathrm{d}t^*(s)}{\mathrm{d}s} \right\} \ge 1 - \alpha \quad s \in [0,S]. \tag{4.17}$$

Proof. For any $\hat{s} \in [0, S]$, if $v(\hat{s})$ satisfies constraint (4.16), then

$$\begin{aligned} 1-\alpha &\leq \text{Prob}\left\{\frac{1}{\min\{v(s), v_{\max}(s)\}} \leq \frac{\mathrm{d}t^*(s)}{\mathrm{d}s},\ \forall s \in [0, S]\right\} \\ &= \text{Prob}\left\{\frac{1}{\min\{v(\hat{s}), v_{\max}(\hat{s})\}} \leq \frac{\mathrm{d}t^*(\hat{s})}{\mathrm{d}s}; \frac{1}{\min\{v(s), v_{\max}(s)\}} \leq \frac{\mathrm{d}t^*(s)}{\mathrm{d}s},\ \forall s \in [0, \hat{s}) \bigcup (\hat{s}, S]\right\} \\ &\leq \text{Prob}\left\{\frac{1}{\min\{v(\hat{s}), v_{\max}(\hat{s})\}} \leq \frac{\mathrm{d}t^*(\hat{s})}{\mathrm{d}s}\right\} \end{aligned}$$

meaning $v(\hat{s})$ also satisfies constraint (4.17). ∎

Constraint (4.17) can be further simplified according to the following proposition.

Proposition 4.3. *Constraint (4.17) is equivalent to the two constraints below,*

$$v(s) \geq \frac{\mathrm{d}t^*(s)}{\mathrm{d}s}, \forall\ s \in [0, S] \tag{4.18}$$

$$\text{Prob}\left\{v_{\max}(s) \geq \frac{\mathrm{d}s}{\mathrm{d}t^*(s)}\right\} \geq 1-\alpha \quad \forall s \in [0, S], \tag{4.19}$$

where $t^*(s)$ satisfies (4.15).

Proof. For any $s \in [0, S]$, constraint (4.17) can be written as

$$\begin{aligned} & \text{Prob}\left\{\min\{v(s), v_{\max}(s)\} \geq \frac{\mathrm{d}s}{\mathrm{d}t^*(s)}\right\} \\ = \quad & \text{Prob}\left\{v(s) \geq \frac{\mathrm{d}s}{\mathrm{d}t^*(s)}, v_{\max}(s) \geq \frac{\mathrm{d}s}{\mathrm{d}t^*(s)}\right\} \geq 1-\alpha. \end{aligned}$$

The proof now follows from the observation that the desired speed $v(s)$ is a deterministic variable and is independent of the random variable $v_{\max}(s)$. ∎

Using the three propositions above, the stochastic optimal speed control model with chance constraints on the journey duration can now be formulated by the objective function (4.8), subject to constraints (4.9), (4.11)–(4.15), (4.18)–(4.19), which we will refer to as StoVer2.

4.2.2 Discretized stochastic nonlinear programming

Using the same discretization described in Section 3.2.1, we divide the road into n segments indexed by $k = 0, 1, ..., n-1$. Define $a_r(k)$ as the actual (constant) acceleration on the segment k, and a new auxiliary variable $\Delta t^*(k)$ that corresponds to the boundary time $\mathrm{d}t^*(s)$ in the original stochastic model for each segment k. A nonlinear programming formulation is then given as follows, which is the discretized version of the StoVer2 (4.8),(4.9), (4.11)–(4.15), (4.18)–(4.19):

$$\underset{a(k)}{\text{Minimize}} \quad \mathbb{E}_{P'} \sum_{k=0}^{n-1} FR\Big(\min\{v(k), v_{\max}(k)\}, a_r(k) \Big) \frac{1}{\min\{v(k), v_{\max}(k)\}} \Delta s \tag{4.20}$$

subject to

$$a_r(k) = \frac{\min\{v(k+1), v_{\max}(k+1)\}^2 - \min\{v(k), v_{\max}(k)\}^2}{2\Delta s} \qquad k \in \{0, 1, ..., n-1\} \tag{4.21}$$

$$a(k) = \frac{v(k+1)^2 - v(k)^2}{2\Delta s} \qquad k \in \{0, 1, ..., n-1\} \tag{4.22}$$

$$a_{\min} \leq a(k) \leq a_{\max} \qquad k \in \{0, 1, ..., n-1\} \tag{4.23}$$

$$v(k) \geq \epsilon \qquad k \in \{1, ..., n-1\} \tag{4.24}$$

$$\sum_{k=0}^{n-1} \Delta t^*(k) = T \tag{4.25}$$

$$v(k)\Delta t^*(k) \geq \Delta s \tag{4.26}$$

$$\text{Prob}\left\{ v_{\max}(k)\Delta t^*(k) \geq \Delta s \right\} \geq 1 - \alpha \qquad k \in \{0, 1, ..., n-1\} \tag{4.27}$$

$$v(0) = v_0, \;\; v(n) = v_S. \tag{4.28}$$

where P' is the probability distribution of the vector $(v_{\max}(0), v_{\max}(1), ..., v_{\max}(n-1))$. When the probability distribution of the traffic speed is known, standard stochastic optimization techniques can be used to solve the model above. The chance constraint (4.27) can be linearized for some particular distributions such as normal and lognormal, or approximated by a convex constraint (Nemirovski and Shapiro 2007). As for the objective function (4.20), it is possible to approximate it using sample average approximation (SAA) (Shapiro et al., 2009) by generating N random traffic speed samples $\xi_i(k)$, $i = 0, 1, ..., N-1$, for each segment $k = 0, 1, ..., n-1$ using the Monte Carlo method satisfying Assumption 4.1, which results in the following formulation:

$$\underset{a(k)}{\text{Minimize}} \quad \frac{1}{N} \sum_{i=0}^{N-1} \sum_{k=0}^{n-1} FR\Big(\min\{v(k), \xi_i(k)\}, a_{ri}(k) \Big) \frac{1}{\min\{v(k), \xi_i(k)\}} \Delta s \tag{4.29}$$

subject to

$$a_{ri}(k) = \frac{\frac{1}{2}\min\{v(k+1), \xi_i(k+1)\}^2 - \frac{1}{2}\min\{v(k), \xi_i(k)\}^2}{\Delta s} \qquad k \in \{0, 1, ..., n-1\}, \; i \in \{0, 1, ...N-1\} \tag{4.30}$$

(4.22)–(4.28).

The nonlinear expression $\min\{v(k), \xi_i(k)\}$ in (4.29) can be linearized by using a continuous variable $v_{r,i}(k)$ and a binary variable $y_i(k)$, subject to the following constraints:

$$v_{r,i}(k) \leq \xi_i(k) \tag{4.31}$$
$$v_{r,i}(k) \leq v(k) \tag{4.32}$$
$$\xi_i(k) - M(1 - y_i(k)) \leq v_{r,i}(k) \leq \xi_i(k) + M(1 - y_i(k)) \tag{4.33}$$
$$v(k) - My_i(k) \leq v_{r,i}(k) \leq v(k) + My_i(k) \tag{4.34}$$
$$y_i(k) \in \{0, 1\}, \tag{4.35}$$

where M is a big constant. The final form of the discretized stochastic NLP is (4.22)–(4.28), (4.29)–(4.35), where $\min\{v(k), \xi_i(k)\}$ in (4.29) and (4.30) is replaced by $v_{ri}(k)$ for each $i = 0, 1, ..., N-1$ and $k = 0, 1, ..., n-1$. Note that this final form is based on the formulation using the relaxed chance constraint (4.17).

4.2.3 Stochastic mixed integer programming

In this part, we transform the model (4.20)–(4.28) to a stochastic MIP, following the same development in Section 3.2.2. By defining new variables $E_r(k) = \min\{E(k), \frac{1}{2}v_{\max}(k)^2\}$ for each $k = 0, 1, ..., n-1$, and denoting P^* as the probability distribution of the vector $\left(v_{\max}(0)^2, v_{\max}(1)^2, ..., v_{\max}(n-1)^2\right)$, we have the following formulation:

$$\underset{a(k)}{\text{Minimize}} \quad \mathbb{E}_{P^*} \sum_{k=0}^{n-1} FR\Big(\sqrt{2E_r(k)}, a_r(k)\Big) f_{PWA}(E_r(k))\Delta s \tag{4.36}$$

subject to

(3.21)–(3.32)

$$
\begin{aligned}
f_{\mathrm{PWA}}(E_r(k)) = {} & (\lambda_2 - \lambda_3) z_{2r}(k) + (\lambda_1 - \lambda_2 + \lambda_3) z_{3r}(k) \\
& - \gamma_3 \delta_{1r}(k) + (\gamma_2 - \gamma_3)\delta_{2r}(k) + (\gamma_1 - \gamma_2 + \gamma_3)\delta_{3r}(k) \\
& - \lambda_3 z_{1r}(k) + \lambda_3 E_r(k) + \gamma_3 \qquad k \in \{0, 1, ..., n-1\}
\end{aligned} \tag{4.37}
$$

$$E_r(k) \le (E_{\max} - E_1)(1 - \delta_{1r}(k)) + E_1 \qquad k \in \{0, 1, ..., n-1\} \tag{4.38}$$

$$E_r(k) \ge E_1 + \varepsilon + (E_{\min} - E_1 - \varepsilon)\delta_{1r}(k) \qquad k \in \{0, 1, ..., n-1\} \tag{4.39}$$

$$E_r(k) \le (E_{\max} - E_2)(1 - \delta_{2r}(k)) + E_2 \qquad k \in \{0, 1, ..., n-1\} \tag{4.40}$$

$$E_r(k) \ge E_2 + \varepsilon + (E_{\min} - E_2 - \varepsilon)\delta_{2r}(k) \qquad k \in \{0, 1, ..., n-1\} \tag{4.41}$$

$$z_{jr}(k) \le E_{\max}\delta_{jr}(k) \qquad j \in \{1, 2, 3\} \qquad k \in \{0, 1, ..., n-1\} \tag{4.42}$$

$$z_{jr}(k) \ge E_{\min}\delta_{jr}(k) \qquad j \in \{1, 2, 3\} \qquad k \in \{0, 1, ..., n-1\} \tag{4.43}$$

$$z_{jr}(k) \le E_j(k) - E_{\min}(1 - \delta_{jr}(k)) \qquad j \in \{1, 2, 3\} \qquad k \in \{0, 1, ..., n-1\} \tag{4.44}$$

$$z_{jr}(k) \ge E_j(k) - E_{\max}(1 - \delta_{jr}(k)) \qquad j \in \{1, 2, 3\} \qquad k \in \{0, 1, ..., n-1\} \tag{4.45}$$

$$-\delta_{1r}(k) + \delta_{3r}(k) \le 0 \qquad k \in \{0, 1, ..., n-1\} \tag{4.46}$$

$$-\delta_{2r}(k) + \delta_{3r}(k) \le 0 \qquad k \in \{0, 1, ..., n-1\} \tag{4.47}$$

$$\delta_{1r}(k) + \delta_{2r}(k) - \delta_{3r}(k) \le 1 \qquad k \in \{0, 1, ..., n-1\} \tag{4.48}$$

$$\delta_{1r}(k), \delta_{2r}(k), \delta_{3r}(k) \in \{0, 1\} \qquad k \in \{0, 1, ..., n-1\} \tag{4.49}$$

$$a_r(k) = \frac{E_r(k+1) - E_r(k)}{\Delta s} \qquad k \in \{0, 1, ..., n-1\} \tag{4.50}$$

$$a(k) = \frac{E(k+1) - E(k)}{\Delta s} \qquad k \in \{0, 1, ..., n-1\} \tag{4.51}$$

$$a_{\min} \le \ a(k) \ \le \ a_{\max} \qquad k \in \{0, 1, ..., n-1\} \tag{4.52}$$

$$E(k) \ge \epsilon \qquad k \in \{1, 2, ..., n-1\} \tag{4.53}$$

$$E(0) = \frac{1}{2} v_0^2, \ E(n) = \frac{1}{2} v_S^2 \tag{4.54}$$

$$\sum_{k=0}^{n-1} \Delta t^*(k) = T \tag{4.55}$$

$$\sqrt{2E(k)}\Delta t^*(k) \ge \Delta s \Leftrightarrow f_{PWA}(E(k)) \le \frac{\Delta t^*(k)}{\Delta s} \qquad k \in \{0, 1, ..., n-1\} \tag{4.56}$$

$$\mathrm{Prob}\left\{ v_{\max}(k)\Delta t^*(k) \ge \Delta s \right\} \ge 1 - \alpha \qquad k \in \{0, 1, ..., n-1\} \tag{4.57}$$

The model above is a stochastic MIP that has a nonlinear objective function with expectation on random vector $\left(v_{\max}(0)^2, v_{\max}(1)^2, ..., v_{\max}(n-1)^2\right)$, and chance constraints (4.57). The expectation in the objective function (4.36) can be handled in the same way as in Section 4.2.2, and linearized for particular fuel consumption models following the same development in Section 3.2.2.

5 Distributionally robust stochastic optimal speed control

The stochastic speed control models presented in the previous section assumed that the probability distribution P underlying the traffic speeds is known with certainty. If the true distribution is not known, or its parameters are uncertain, then the resulting solutions of the stochastic optimization models may be suboptimal. In order to allow for any uncertainty in the forms or parameters of the probability distribution, we resort to the use of uncertainty sets in the stochastic optimization formulations in Section 4 that will provide for distributional robustness (Ben-Tal et al., 2009).

In formal terms, let Φ be the nominal distribution that is a best estimate of the true (but unknown) distribution P of the traffic speeds over the whole journey. The structure of Φ can be different to that of P, and it can be obtained via many ways such as Bayesian estimation method (Park et al., 2010). We then define an ambiguity set $\mathbb{P}$ as follows:

$$\mathbb{P} = \{\Phi' \in \mathbb{D} : D(\Phi'||\Phi) \leq \eta\}, \tag{5.1}$$

where $\mathbb{D}$ denotes the set of probability distributions, $D(\Phi'||\Phi) = \int_V \phi(x)\log\frac{\phi(x)}{\phi'(x)}\mathrm{d}x$ is the "distance" between distributions Φ' and Φ (with V representing the range of variable x, and $\phi(x)$ and $\phi'(x)$ being the probability mass functions of Φ' and Φ, respectively), and η is a positive constant that controls the size of the ambiguity set $\mathbb{P}$. Note that the ambiguity set $\mathbb{P}$ covers a wider range of traffic speeds than the nominal distribution Φ, where the range depends on the value of η. There are different ways to measure the distance between two probability distributions. The expression (5.1) that we use here is based on the method proposed by Hu and Hong (2013) where the ambiguity set is defined by the Kullback-Leibler (KL) divergence. Next, we show how to incorporate distributional robustness into the two stochastic optimal control models with chance constraints described in Section 4.

5.1 Robust chance constraints on the vehicle speed

We revisit the formulations described in Section 4.1, where the chance constraints (4.1) are replaced with the following expression that considers all distributions in the ambiguity set $\mathbb{P}$ with probability $1-\alpha$:

$$\mathrm{Prob}_{\Phi'}\left\{v(s) \leq v_{\max}(s)\right\} \geq 1-\alpha \quad \forall \Phi' \in \mathbb{P}, s \in [0, S], \tag{5.2}$$

which, according to Theorem 8 in Hu and Hong (2013), is equivalent to:

$$\mathrm{Prob}_{\Phi}\{v(s) \leq v_{\max}(s)\} \geq 1-\bar{\alpha} \quad \forall s \in [0, S], \tag{5.3}$$

where

$$\bar{\alpha} = \sup_{z>0} \frac{e^{-\eta}(z+1)^{\alpha} - 1}{z}. \tag{5.4}$$

According to Hu and Hong (2013), the new parameter $\bar{\alpha}$ can be easily calculated via bisection search Algorithm 1.

Algorithm 1: Calculation of $\tilde{\alpha}$.

Initialization: Set $j = 0$, $\alpha_l := 0$ and $\alpha_u := \alpha$

Step j: Set $\tilde{\alpha} = (\alpha_l + \alpha_u)/2$

- If $H(z^*(\tilde{\alpha})) > 0$, update $\alpha_l := \tilde{\alpha}$. Set $j = j + 1$.
- If $H(z^*(\tilde{\alpha})) < 0$, update $\alpha_u := \tilde{\alpha}$. Set $j = j + 1$.
- If $H(z^*(\tilde{\alpha})) = 0$, stop and return $\tilde{\alpha}$.

In Algorithm 1,

$$H(z) = e^{-\eta}(z+1)^{\alpha} - 1 - \tilde{\alpha}z$$

$$z^*(\tilde{\alpha}) = \max\left\{0, \left(\frac{\tilde{\alpha}e^{\eta}}{\alpha}\right)^{\frac{1}{\alpha-1}} - 1\right\}.$$

The resulting robust optimal control model with the speed chance constraints (5.3) and (5.4) can be solved either as a NLP or as a MIP, in the same way as described in Section 4.1, to which we will refer as RStoVer1.

5.2 Robust chance constraints on the journey duration

Extending the formulation in Section 4.2.1 to account for distributional robustness requires a change in both the objective function (4.8) and the chance constraint (4.19). In the objective function, the distributionally robust control should minimize the worst case of the expected fuel consumption along the journey under all possible distributions as follows:

$$\underset{a(s)}{\text{Minimize}} \ \underset{\Phi' \in \mathbb{P}}{\text{Maximize}} \quad \mathbb{E}_{\Phi'} \int_0^S FR(\min\{v(s), v_{\max}(s)\}, a_r(s)) \frac{1}{\min\{v(s), v_{\max}(s)\}} \mathrm{d}s, \tag{5.5}$$

where the maximum is taken with respect to all distributions in the ambiguity set. Invoking Theorem 4 in Hu and Hong (2013), the objective function (5.5) is equivalent to the following one:

$$\underset{v(s), u \geq 0}{\text{Minimize}} \quad u \log \mathbb{E}_{\Phi} e^{\left[\frac{1}{u}\int_0^S FR(\min\{v(s), v_{\max}(s)\}, a_r(s)) \frac{1}{\min\{v(s), v_{\max}(s)\}} \mathrm{d}s\right]} + u\eta. \tag{5.6}$$

Similarly, the chance constraint (4.19) is modified so that it is satisfied over all distributions in the ambiguity set $\mathbb{P}$, as shown below:

$$\text{Prob}_{\Phi'}\left\{v_{\max}(s)\mathrm{d}t^*(s) \geq \mathrm{d}s\right\} \geq 1-\alpha \quad \forall \Phi' \in \mathbb{P}, s \in [0, S], \tag{5.7}$$

which, resorting once again to Theorem 8 in Hu and Hong (2013), is equivalent to:

$$\text{Prob}_{\Phi}\left\{v_{\max}(s)\mathrm{d}t^*(s) \geq \mathrm{d}s\right\} \geq 1-\bar{\alpha} \quad \forall s \in [0, S], \tag{5.8}$$

where $\bar{\alpha}$ is given earlier in Eq. (5.4). The resulting distributionally robust formulation can now be stated as (5.6), (5.8), (4.9), (4.11)–(4.15), (4.18), to which we will refer as RStoVer2. This formulation can be converted into a MIP and solved with nonlinear integer programming software.

6 Case study

This section undertakes the computational tests to numerically investigate the models developed in the paper. The aim of the experimentation is four-fold. First, we test the performance of alternative solution methods on solving the deterministic optimal control problem in order to identify the best method to use for the stochastic models. Second, we assess the performance of the stochastic models and quantify the value of considering the stochasticity in the traffic speed. Third, we evaluate the impact of the traffic speed uncertainty on the journey time and fuel consumption. Finally, we investigate the benefits of incorporating distributional robustness into the models. The findings are presented in Sections 6.1–6.5, corresponding to the four aims, respectively. In all the experiments, we use the CMEM to calculate the vehicle fuel consumption, the details of which are given in Appendix.A.

Unless specified otherwise, the numerical experiments are conducted on an instance with a road section of 600 meters in length, where the road grade and the deterministic traffic speeds along the road are shown in Figures 2 and 3, respectively. The instance assumes 3 m/s^2 as maximum acceleration, 4 m/s^2 as maximum deceleration, and 3 m/s as initial and terminal speeds. The journey time is limited to 61 seconds, and the whole trip is divided into 30 segments, with 20 meters per segment. All models and solution algorithms are implemented and run on a MacBook Pro with 2.4 GHz CPU and 8 GB memory.

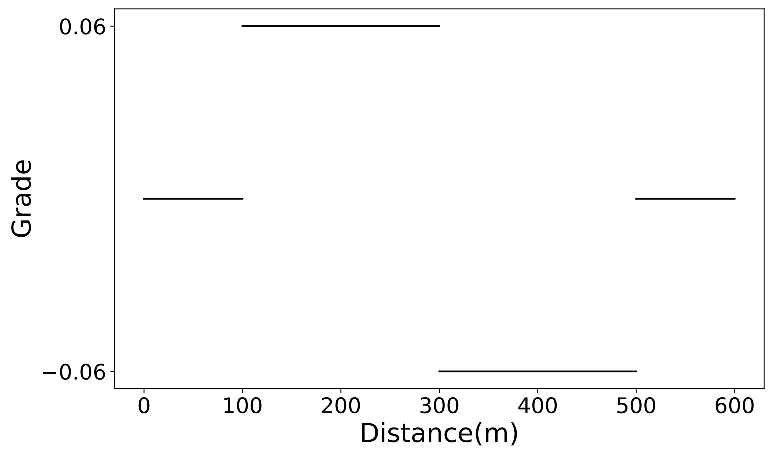

Figure 2: The grade of the terrain in the instance

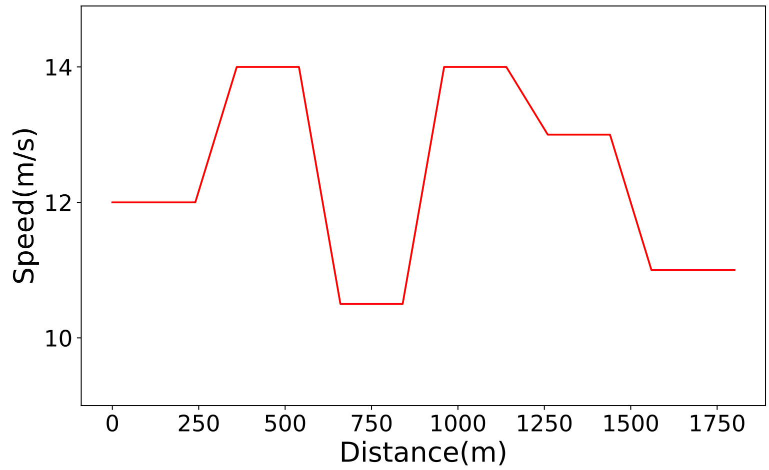

Figure 3: Traffic speeds used in the instance

6.1 Comparison of solution methods for deterministic optimal control

The solution methods tested in this section include DP (explained in Appendix.B and coded in Python), and the NLP and MILP models are solved using Gurobi Optimizer 9.0. The PWA function used to approximate the curve $\frac{1}{\sqrt{2E}}$ uses 50 segments, covering a speed range from 0 m/s to 20 m/s as shown in Figure 4, with the corresponding unit-mass kinetic energy ranging from 0 m^2/s^2 to 200 m^2/s^2. All intersections between two adjacent pieces are chosen to be the points on the curve $\frac{1}{\sqrt{2E}}$ and have evenly distributed horizontal coordinates.

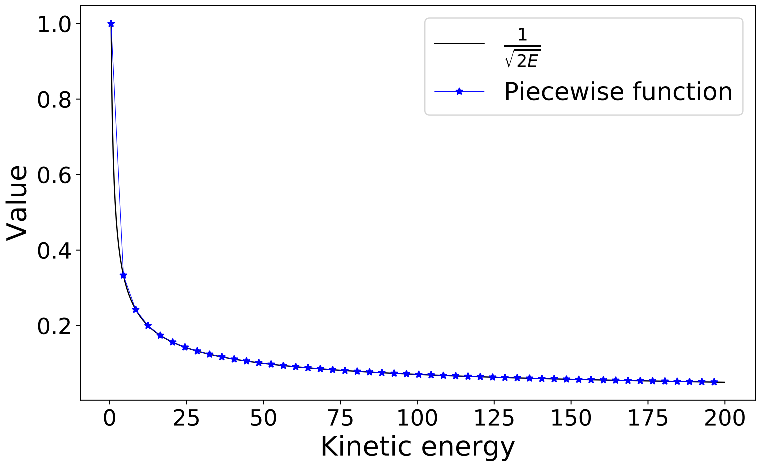

Figure 4: Piecewise function used in the experiments

The results yielded by the three methods are presented in Table 1. For comparison, Figures 5 and 6 show the speed and acceleration profiles calculated by the three methods, which are very similar and within the allowable bounds.

Table 1: Performance of different solution methods

Method	Fuel consumption (Gram)	Trip duration (Second)	Calculation Time (Second)
MILP	113.49	60.97	0.30
NLP	113.48	61.00	1338.82
DP	114.10	60.85	62.10

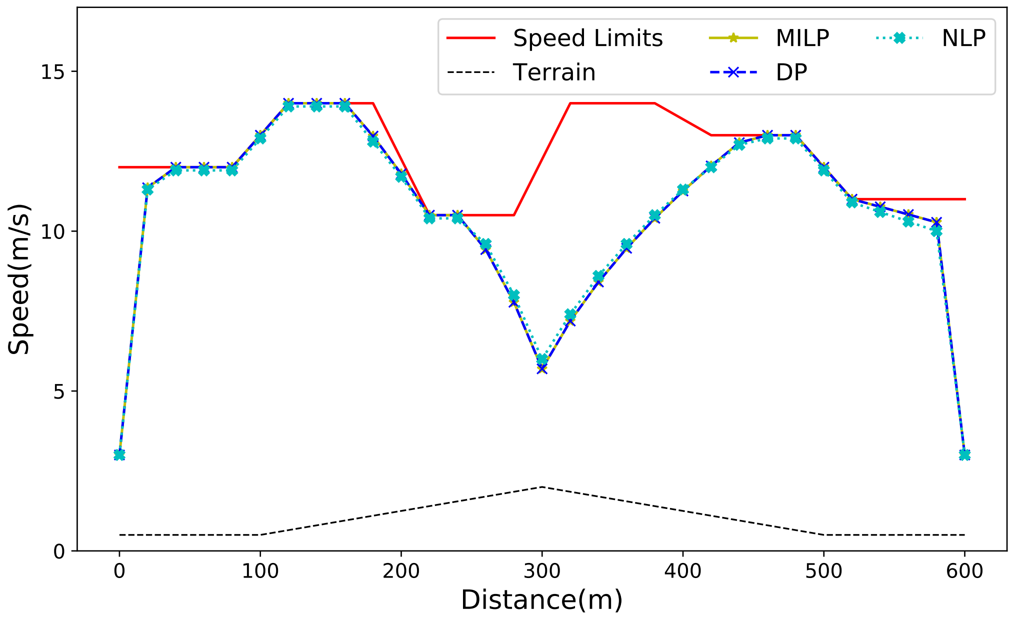

Figure 5: Speed trajectories obtained by the three methods

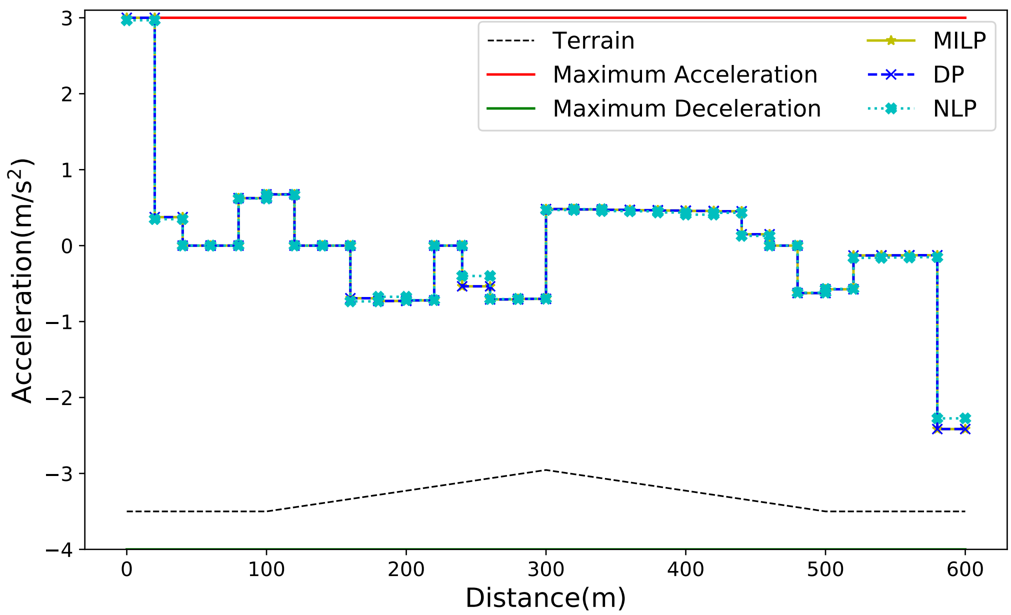

Figure 6: Acceleration profiles obtained by the three methods

The results in Table 1 show that, the three methods yield to similar fuel consumptions and trip durations, but require considerably different computation times. NLP has the best objective value as it uses all travel time budget, at the expense of a very long computation time. DP consumes shorter computation time but yields the highest fuel consumption. MILP has the shortest computation time and performs similar to NLP on fuel consumption and trip duration. Based on the comparison, MILP will be used as the solution method in the remainder of the experiments. We have also tested different discretization levels by using 12, 15 and 20 meters per segment, and found that the resulting amounts of fuel consumption differ only slightly, and at most by 2.45% when compared against a finer level discretization using a segment length equal to 1 meter.

6.2 Performance of the stochastic speed optimal control models

Following Rakha et al. (2006) and Hofleitner et al. (2012) which suggested that the lognormal distribution shows a good fit for travel times and is inversely proportional to vehicle speeds, we model traffic speed $v_{\max}(k)$ for segment k as a lognormal distribution with mean $\mu(k)$ and standard deviation $\sigma(k)$. Then, $\ln(v_{\max}(k))$ is normally distributed with the following mean $\mu_{ln}(k)$ and standard deviation $\sigma_{ln}(k)$:

$$\mu_{ln}(k) = \ln\left(\frac{\mu(k)^2}{\sqrt{\sigma(k)^2 + \mu(k)^2}}\right) \tag{6.1}$$

$$\sigma_{ln}(k) = \sqrt{\ln\left(1 + \frac{\sigma(k)^2}{\mu(k)^2}\right)}. \tag{6.2}$$

In the following experiments, we set $\mu(k)$ equal to the traffic speeds shown in Figure 3, the relative standard deviation RSD $= \sigma(k)/\mu(k) = 0.1$, and increase the time limit to 65 seconds. We test the values of $\alpha \in \{0.02, 0.05, 0.1\}$ in the chance constraints of StoVer1 and StoVer2.

In formulation StoVer1, since $v_{\max}(k)$ follows the lognormal distribution, the speed chance constraint (4.4) can be converted to an explicit form for each $k \in \{1, 2, ..., n-1\}$ as follows,

$$\begin{aligned}
&\text{Prob}\left\{2E(k) \leq v_{\max}(k)^2\right\} \geq 1-\alpha \\
\Longleftrightarrow\ &\text{Prob}\left\{\frac{1}{2}\ln(2E(k)) \leq \ln(v_{\max}(k))\right\} \geq 1-\alpha \\
\Longleftrightarrow\ &\frac{1}{2}\ln(2E(k)) \leq \mu_{ln}(k) + z_\alpha \sigma_{ln}(k) \\
\Longleftrightarrow\ &E(k) \leq \frac{1}{2}e^{2(\mu_{ln}(k)+z_\alpha\sigma_{ln}(k))},
\end{aligned} \tag{6.3}$$

where z_α is the value of the α quantile of the standard normal distribution.

Solving StoVer1 yields the speed profiles in Figure 7 for different values of α. The calculation time is around 0.30s for each α. As the figure shows, when α is reduced, the desired speed is reduced due to the speed chance constraint becoming tighter, except between 300–400 m where the vehicle needs to travel faster to meet the journey time constraint.

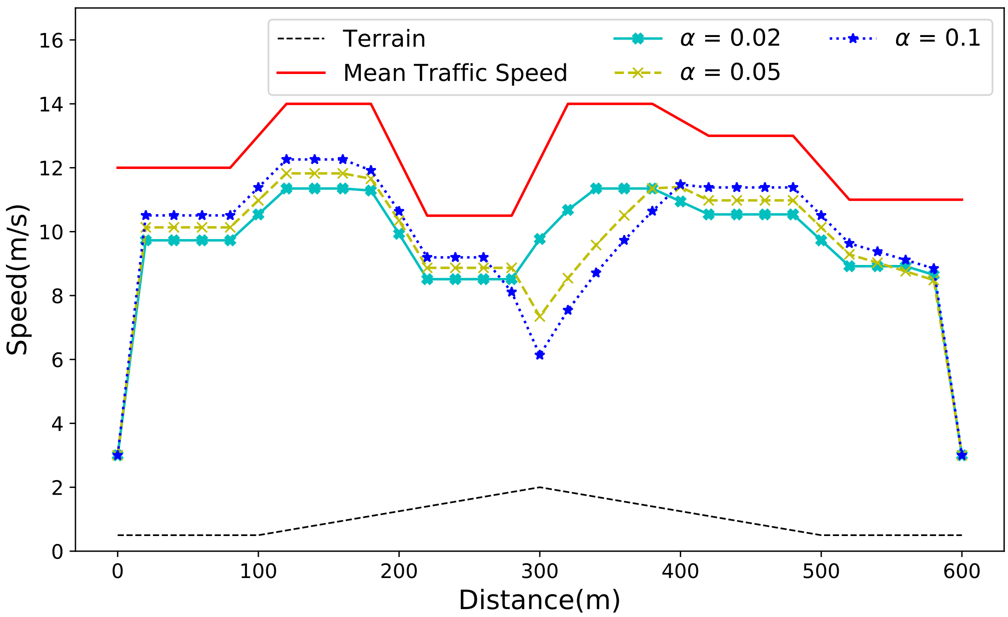

Figure 7: StoVer1 speed trajectories under different α

As for StoVer2, we randomly generate 100 traffic speed scenarios. Each scenario consists of a series of randomly sampled traffic speeds along the journey, one traffic speed per location. While sampling the traffic speeds, we check whether the accelerations between adjacent locations satisfy Assumption 4.1, and continue to resample until they do. Similar to StoVer1, the chance constraint (4.57) can be converted for all $k \in \{1, 2, ..., n-1\}$ as follows:

$$\begin{aligned} & \text{Prob}\left\{v_{\max}(k)\Delta t^*(k) \geq \Delta s\right\} \geq 1 - \alpha \\ \iff & \text{Prob}\left\{v_{\max}(k) \geq \frac{\Delta s}{\Delta t^*(k)}\right\} \geq 1 - \alpha \\ \iff & \Delta s \leq \Delta t^*(k) e^{(\mu_{ln}(k) + z_\alpha \sigma_{ln}(k))}. \end{aligned} \tag{6.4}$$

The results are shown in Figure 8 for $\alpha \in \{0.02, 0.05, 0.1\}$, where the dashed lines are the boundaries of the sampled traffic speeds in the generated scenarios, and between the boundaries each red dot indicates a sampled traffic speed.

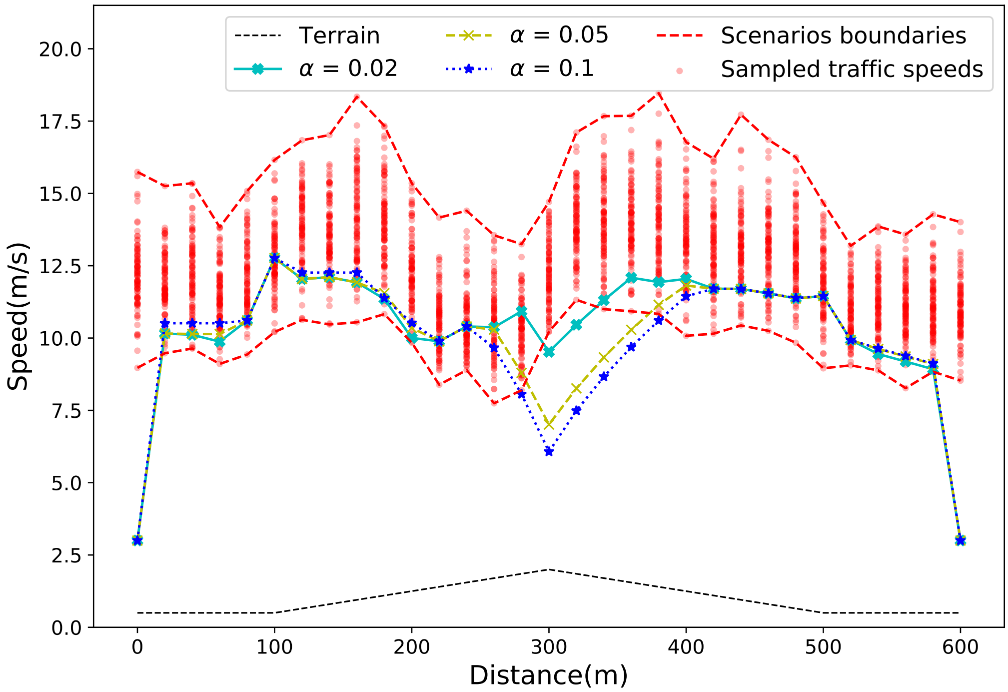

Figure 8: StoVer2 speed trajectories under varying α

As Figure 8 shows, the desired speed trajectories under different values of α do not significantly differ from each other, except between 300–400 m where the desired speed is higher when α is smaller. The computation times for $\alpha \in \{0.02, 0.05, 0.1\}$ are 221s, 262s, 355s, respectively.

6.2.1 The value of stochastic modeling

Next, we quantify the benefit of the stochastic modeling, i.e., treating the uncertainty in the traffic speeds explicitly with the stochastic models as opposed to running the deterministic optimal speed control model using mean traffic speeds. To this end, we simulate the desired speed trajectories obtained by the deterministic model and by the StoVer1 and StoVer2 with 1000 traffic speed scenarios (note that these 1000 scenarios are different from the 100 scenarios used in Section 6.2.1). Given the desired speed trajectories, we then compute the actual trip duration and fuel consumption in each of the 1000 scenarios, where the actual speeds are equal to either the desired speeds or the traffic speeds, whichever is smaller.

To evaluate the performance of the solutions with respect to the chance constraints on the journey duration (4.10), we first restate the constraints as the following function that uses discretization (6.5),

$$\text{Prob}\left\{\sum_{k=0}^{n-1}\frac{\Delta s}{\min\{v(k), v_{\max}(k)\}} \leq T\right\} \geq 1-\alpha, \tag{6.5}$$

and use it to calculate the violation of journey duration constraints.

Figure 9 presents the speed trajectories obtained by different methods using $\alpha = 0.05$. The trajectories given by StoVer1 and StoVer2 are similar, and fluctuate less than the trajectory given by the deterministic method. Figures 10–12 show the distributions of actual fuel consumption and journey durations in the 1000 scenarios. It can be seen that, under the random traffic speeds, the deterministic model yields to a much higher degree of variability in fuel consumption and journey time, in comparison to the stochastic models.

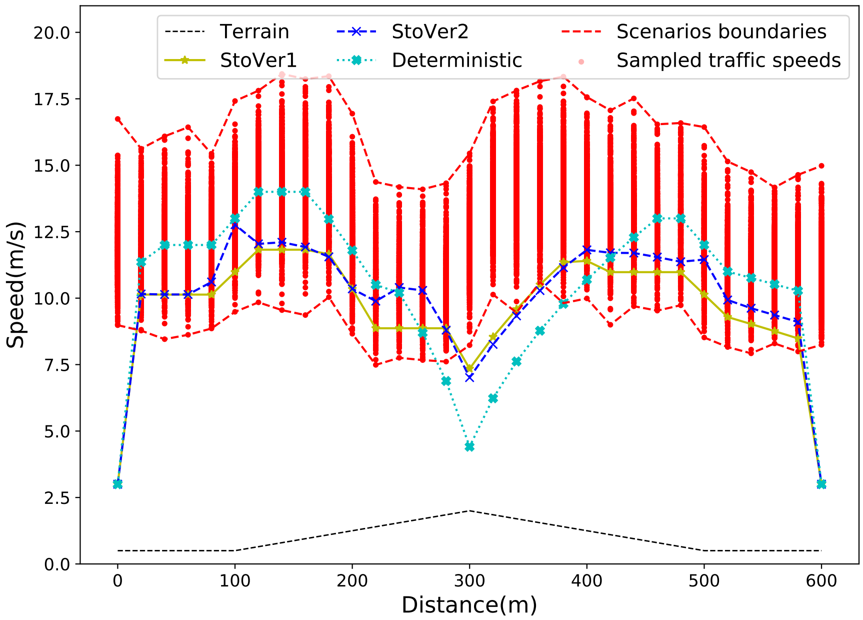

Figure 9: Speed trajectories obtained by the different models for $\alpha = 0.05$

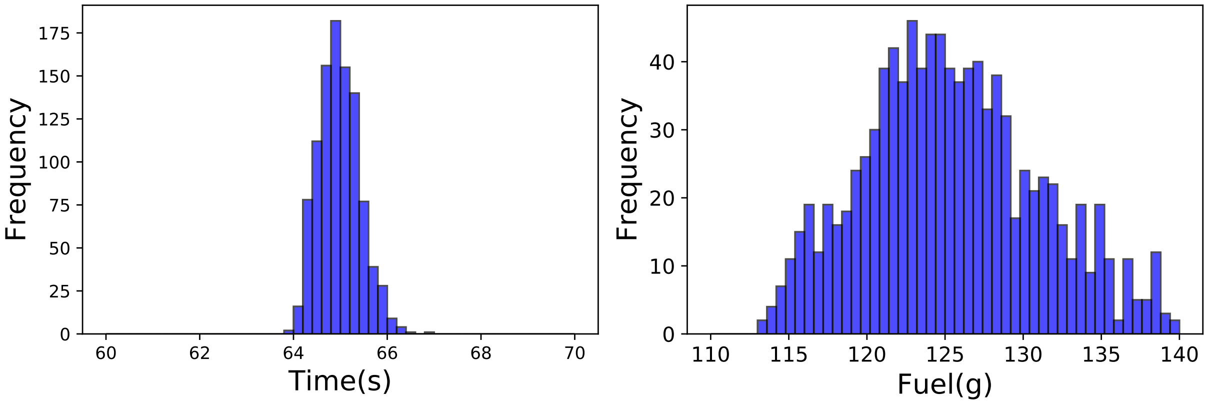

Figure 10: Journey time and fuel consumption of trajectories given by the deterministic model

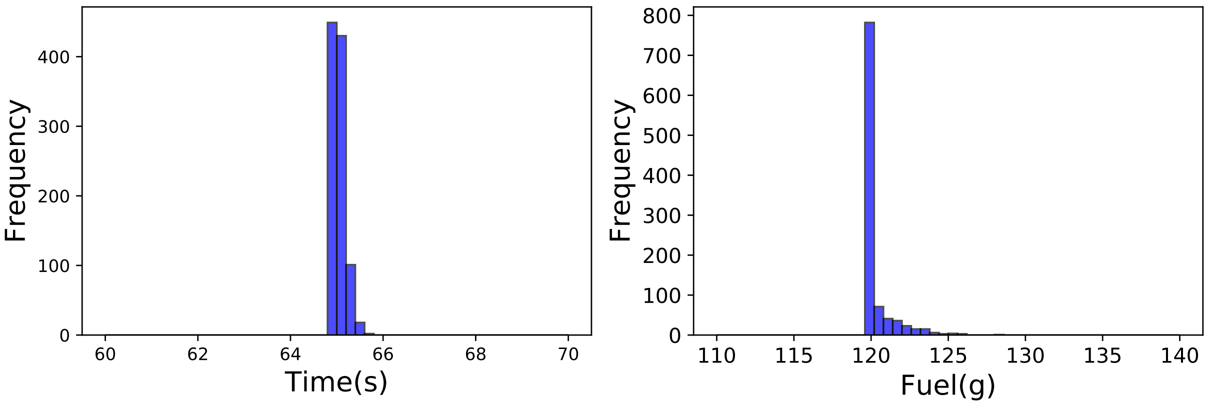

Figure 11: Journey time and fuel consumption of trajectories given by StoVer1 ($\alpha = 0.05$)

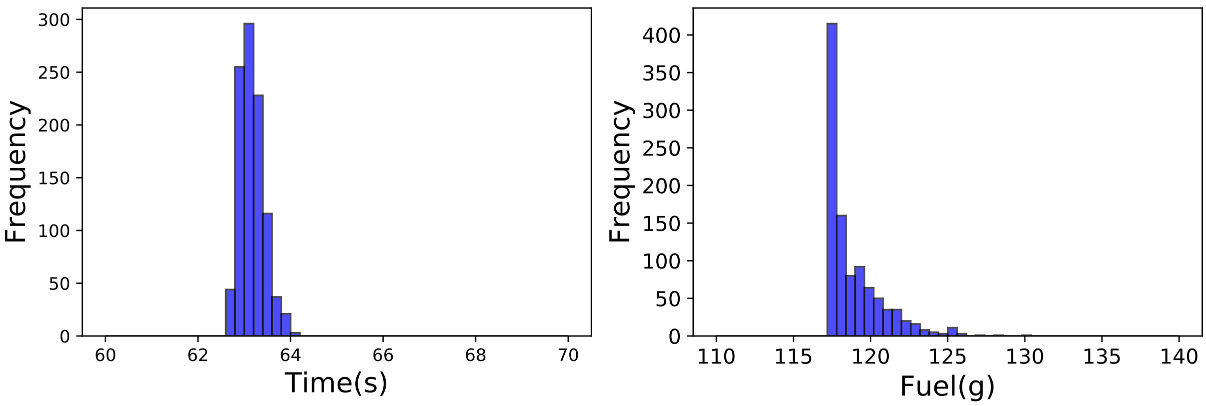

Figure 12: Journey time and fuel consumption of trajectories given by StoVer2 ($\alpha = 0.05$)

Table 2 shows the average fuel consumption resulting from the solutions of the three models under different values of α, indicating that StoVer2 yield lower average fuel consumption than the deterministic version. For the StoVer1 and StoVer2, the average fuel consumption increases as α decreases, due to the solutions becoming more risk-averse.

StoVer2 yields the lowest average fuel consumption for all α. StoVer1 leads to lower average fuel consumption than the deterministic model when $\alpha = 0.05, 0.1$, and higher when $\alpha = 0.02$.

Tables 3 and 4 show the percentage of the 1000 scenarios in which the planned speed profiles exceed traffic speeds on at least one segment and when the journey time limit is violated, respectively. In Table 3, the trajectories computed by StoVer1 violate the traffic speed the least, mainly because it is designed to limit the traffic speed violation. The deterministic model yields to a much more frequent violation in traffic speeds than the two stochastic models.In Table 4, StoVer2 performs the best in on-time arrival than other models: 100% on time when $\alpha = 0.02$ and $\alpha = 0.05$, and 98.7% when $\alpha = 0.1$, as the formulation is designed to limit the probability of late arrival at the destination. The deterministic model, and StoVer1 with large α, lead to much higher degrees of late arrival.

Table 2: Average fuel consumption (Gram) over 1000 scenarios

α	Deterministic	StoVer1	StoVer2
0.02	126.01	129.94	125.46
0.05	126.01	120.27	118.88
0.10	126.01	117.88	117.50

Table 3: Percentage of speed violations over 1000 scenarios

α	Deterministic	StoVer1	StoVer2
0.02	29.88%	1.70%	14.14%
0.05	29.88%	3.50%	11.78%
0.10	29.88%	6.57%	11.65%

Table 4: Percentage of journey time violations over 1000 scenarios

α	Deterministic	StoVer1	StoVer2
0.02	48.90%	35.00%	0
0.05	48.90%	55.60%	0
0.10	48.90%	78.20%	1.30%

6.2.2 Comparison of the stochastic model and reactive model

To show the benefits that our stochastic models can bring over reactive methods, we modify the look-ahead control method in Hellström et al. (2009) as described below, and use as a reactive control mechanism.

$$\underset{a(s)}{\text{Minimize}} \quad \int_{S_k}^{S_k+d_l} FR(v(s), a(s)) \frac{1}{v(s)} \mathrm{d}s + \beta \int_{S_k}^{S_k+d_l} \frac{1}{v(s)} \mathrm{d}s \tag{6.6}$$

subject to

$$a(s) = \frac{\mathrm{d}v(s)^2}{2\mathrm{d}s} \qquad s \in [S_k, S_k + d_l] \tag{6.7}$$

$$a_{\min} \leq a(s) \leq a_{\max} \qquad s \in [S_k, S_k + d_l] \tag{6.8}$$

$$\epsilon \leq v(s) \leq v_{\max}(s) \qquad s \in [S_k, S_k + d_l] \tag{6.9}$$

$$v(S_k) = v_{S_k}, \tag{6.10}$$

where S_k is the distance from the origin to present location, d_l is the distance of look-ahead horizon, v_{S_k} is the vehicle speed at the present location, β is a scalar factor which can be tuned to balance the trade-off between the fuel consumption and journey time.

The way that the reactive control machanism operates is illustrated in Figure 13, which shows a vehicle moving from segment k to segment $k+1$. The whole journey is divided into n segments of length Δs as described in subsection 3.2.1, where the beginning of each segment is a point where the reactive control will be executed. As the vehicle is en-route towards the destination, it will replan the speed profile over the look-ahead horizon $[S_k, S_k + d_l]$ at each replanning point S_k using the deterministic model (6.6)–(6.10). The traffic speeds from S_k to $S_k + d_l$ are assumed to be the realized speeds. When the vehicle runs following the replanned speed profile and arrives at the subsequent replanning point S_{k+1}, the traffic speeds in the new look-ahead horizon $[S_{k+1}, S_{k+1} + d_l]$ will be known and thus the trajectory will be replanned.

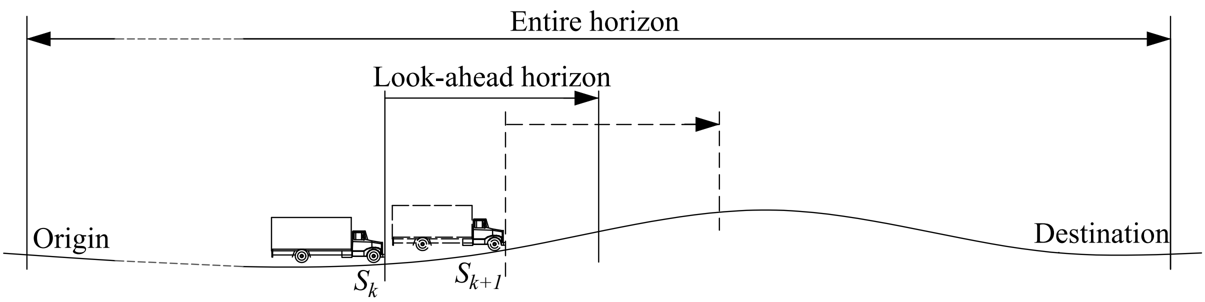

Figure 13: Illustration of the reactive control

The reactive control model (6.6)–(6.10) uses the realized traffic speeds to guarantee the feasibility of its planning speeds, so it is impractical to compare it with StoVer1. To compare the reactive control model and StoVer2, we use a different instance with a longer journey (a 5000 meters road, the grade is shown in Figure 14), where the mean traffic speeds are shown in Figure 15 with $RSD = 0.15$, and the journey time is set to be limited to 370 seconds.

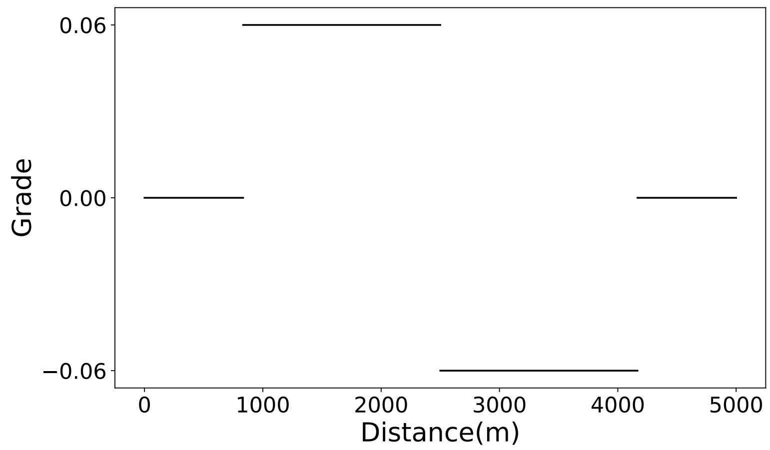

Figure 14: The grade of terrain terrain over the journey

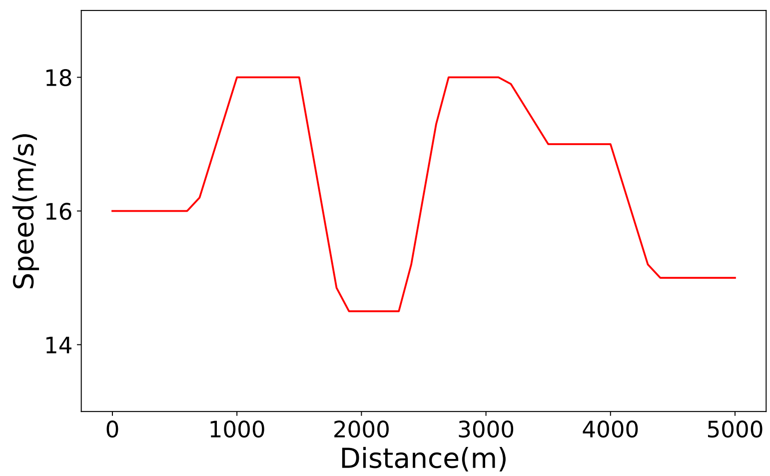

Figure 15: The mean traffic speeds over the journey

For the comparison, we first generate 1000 traffic speed scenarios along the journey, and investigate the performance of StoVer2 as in subsection 6.2.1. The results are shown as the red scatters in Figure 16, where the five points correspond to $\alpha \in \{0.28, 0.29, 0.30, 0.31, 0.32\}$. Then we run the reactive control model 1000 times, each time under one of the 1000 scenarios. The average fuel consumption and the percentage of time violation given by the reactive control model under six different lengths of the look-ahead horizon, namely 300, 700, 1100, 1900, 2700, 3500 meters, are shown by the lines in Figure 16, where the points on each line (from right to left) correspond to $\beta \in \{0, 0.5, 1, 1.5, 2, 2.5, 3, 3.5, 4, 4.5\}$. When β increases, the percentage of time violation decreases, which is intuitive because increasing the value of β can lead to giving a larger weight to the journey time. In addition, the length of the look-ahead horizon can significantly affect the performance of the reactive control model, and it is difficult to decide the optimal length. For illustration, we fix the value $\beta = 1$ and use different look-ahead horizons, and the calculation results are given in Figure 17. It is revealed that a setting of $d_l = 700m$ is needed to minimize the total fuel consumption, $d_l = 2300m$ to minimize time violation, and $d_l = 1100m$ to balance both performance measures.

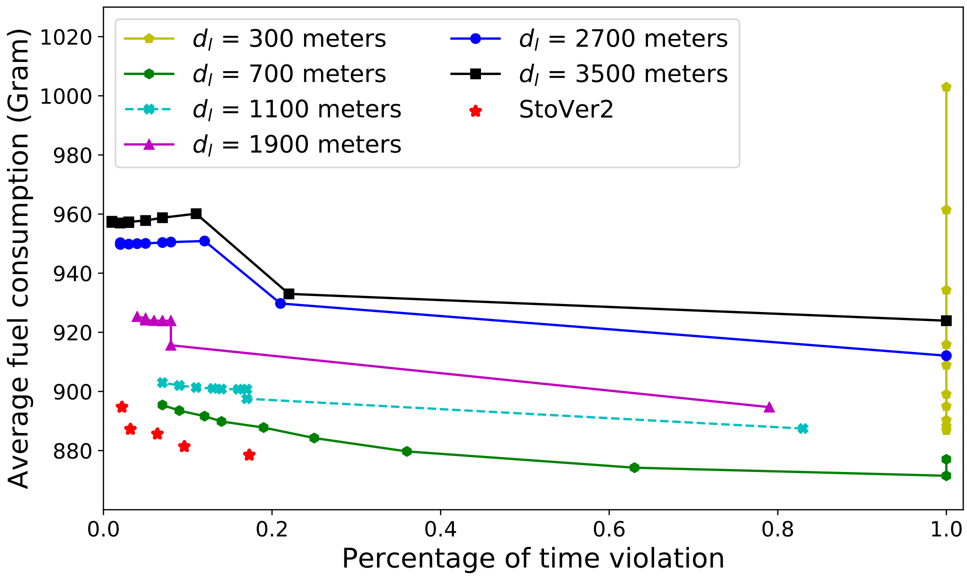

Figure 16: The fuel consumption and percentage of time violation of StoVer2 and reactive control model

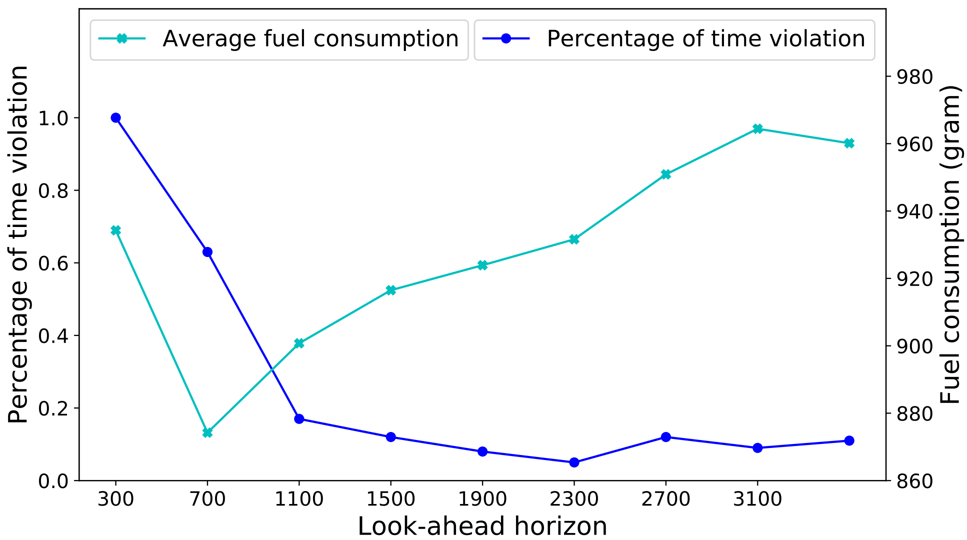

Figure 17: The percentage of time violation and fuel consumption of reactive control model under different look-ahead horizons

As Figure 16 shows, considering the two criteria (fuel consumption and percentage of time violation), the solutions of StoVer2 dominate most solutions provided by the reactive control model. And the speed profiles yielded by StoVer2 require less fuel consumption as compared to those of the reactive control model implemented here under the same percentage of time violation. These results suggest that StoVer2 has an obvious advantage over the reactive control as implemented in this paper.

6.3 The impact of the traffic speed variability

In this section, we investigate the impact of the variation in traffic speeds on fuel consumption and solution feasibility, and then on the planned speed profiles, when using StoVer1 and StoVer2.

6.3.1 Fuel consumption and solution feasibility

For the experiments below, we use a time limit of $T = 65$ seconds, set $\alpha = 0.05$, and use the mean traffic speeds shown in Figure 3. Different values of RSD $\in \{0.01, 0.04, 0.07, 0.10, 0.15\}$ are used to investigate the impact of traffic speed standard deviation on the model performances. The resulting trajectories are then simulated under the 1000 test scenarios as in the previous section.

The trajectories resulted from StoVer1 for RSD $= 0.04$, 0.07 and 0.10 are shown in Figure 18. When RSD increases, the speed chance constraint will get tighter, and lower desired speeds are observed over most parts of the journey, except between 300–400 m as in previous sections. The average fuel consumption underdifferent values of α and RSD are shown in Table 5, where NaN indicates that the model was infeasible due to the chance constraint, and the last row shows the results of the deterministic model based on mean traffic speed. Similarly, Table 6 shows the percentage of the 1000 scenarios in which the planned speed profiles exceed the traffic speeds and when the journey time limit is violated. The results collectively indicate that the fuel consumption and percentage of speed violation both increase with RSD. Although StoVer1 does not necessarily lead to lower fuel consumption, it reduces the infeasible solutions caused by unattainable speeds.

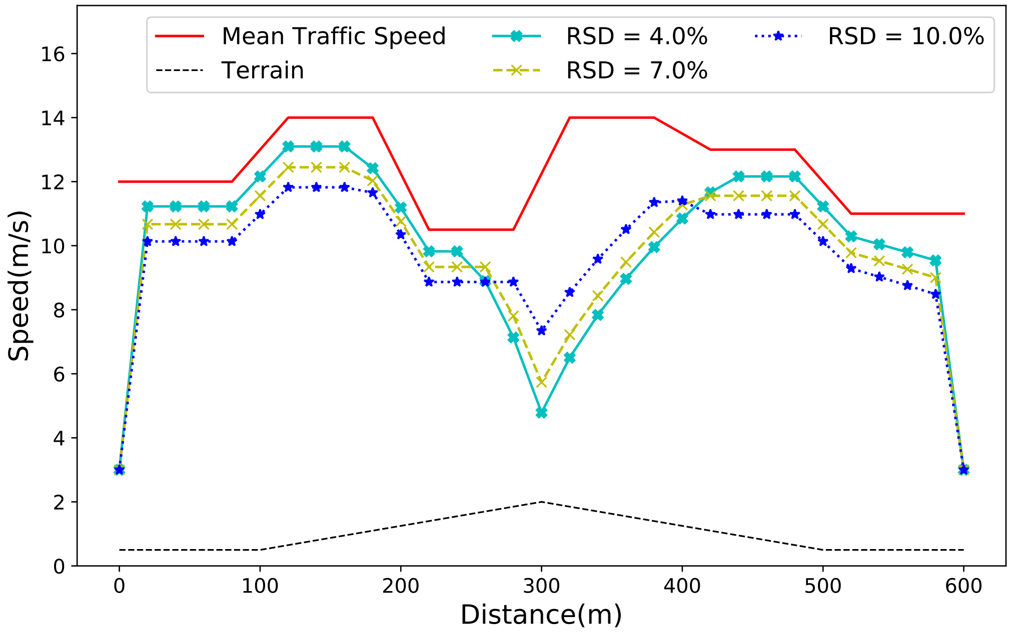

Figure 18: StoVer1 speed trajectories under varying RSDs ($\alpha = 0.05$)

Table 5: Average fuel consumption (Gram) of StoVer1 speed profiles over 1000 scenarios

	Relative standard deviation (RSD)				
α	0.01	0.04	0.07	0.10	0.15
0.02	113.23	114.56	117.66	129.91	NaN
0.05	113.18	114.20	116.12	120.22	NaN
0.10	113.15	114.03	115.48	117.79	128.90
0.15	113.14	114.04	115.48	117.36	122.86
0.20	113.15	114.13	115.76	117.66	122.22
Deterministic	113.30	115.76	120.14	125.36	135.99

Table 6: Percentage of speed violations in StoVer1 speed profiles over 1000 scenarios

	Relative standard deviation (RSD)				
α	0.01	0.04	0.07	0.10	0.15
0.02	0.75%	0.98%	1.23%	1.78%	NaN
0.05	1.97%	2.51%	2.91%	3.63%	NaN
0.10	3.95%	4.98%	5.68%	6.54%	8.66%
0.15	5.85%	7.26%	8.27%	9.50%	11.51%
0.20	7.60%	9.43%	11.04%	12.40%	14.34%
Deterministic	19.49%	23.35%	26.52%	29.71%	33.52%

Similar results for StoVer2 are shown in Figure 19 and Tables 7 and 8. The trend in the speed profiles is similar to StoVer1, but StoVer2 always yields lower fuel consumption in comparison to the deterministic model even under small values of α. The journey time limit is violated more often as the traffic speed variability (RSD) and α increase. This is caused by the relaxed time chance constraint (4.19) and a larger variance in the generated scenarios for larger values of RSD.

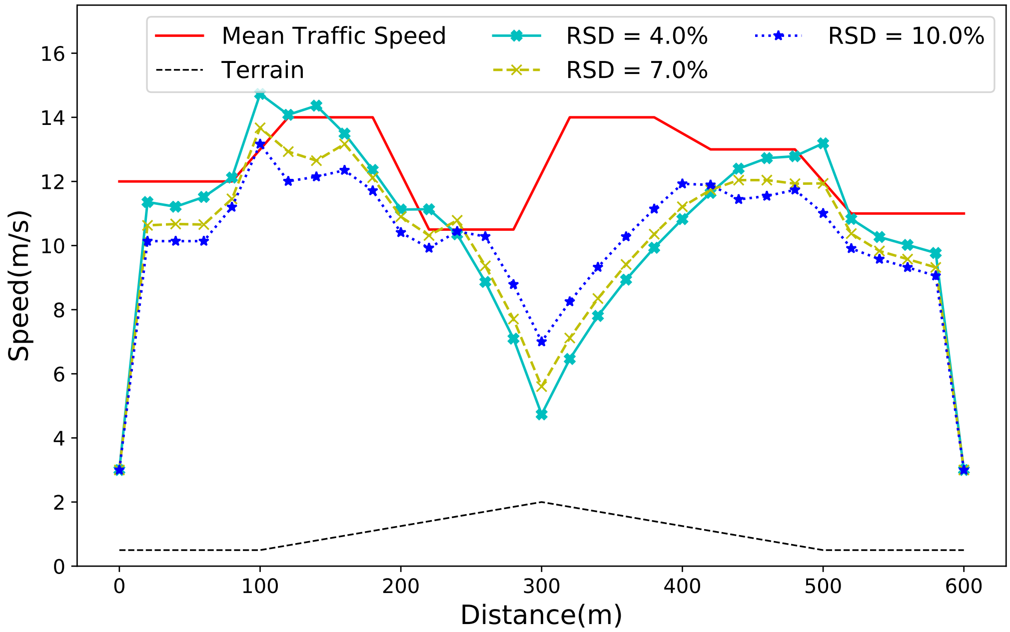

Figure 19: StoVer2 speed trajectories under varying RSDs ($\alpha = 0.05$)

Table 7: Average fuel consumption (Gram) of StoVer2 speed profiles over 1000 scenarios

	Relative standard deviation (RSD)				
α	0.01	0.04	0.07	0.10	0.15
0.02	113.04	113.91	116.22	125.39	NaN
0.05	113.04	113.87	115.52	118.83	NaN
0.10	113.04	113.80	115.33	117.48	126.88
0.15	113.03	113.83	115.16	116.99	122.53
0.20	113.04	113.80	115.09	116.92	121.88
Deterministic	113.32	115.81	120.22	125.82	135.70

Table 8: Percentage of journey time violations in StoVer2 speed profiles over 1000 scenarios

	Relative standard deviation (RSD)				
α	0.01	0.04	0.07	0.10	0.15
0.02	0	0	0	0	NaN
0.05	0	0	0	0	NaN
0.10	0	0	0.3%	1.5%	1.0%
0.15	0	0.1%	2.3%	12.2%	34.9%
0.20	0	2.3%	13.3%	58.1%	76.9%
Deterministic	0	0	4.80%	46.8%	89.9%

6.3.2 Variability in the planned speed profiles

A potential user of the results may wonder how the planned speed profiles change as traffic conditions vary. To answer this question, we use a simplified instance that assumes a flat terrain, a road length of 600 m, and a mean traffic speed equal to 15.5 m/s over the entire journey. For a fixed journey duration equal to $T = 65$ seconds and assuming zero acceleration, the function that represents the CMEM model used to calculate the total fuel consumption (Appendix A) is minimized when the (constant) vehicle speed is around 15.28 m/s (Demir et al., 2014), to which the initial and terminal speeds are set equal. This speed results in a journey duration of 38 seconds which is well within the time limit. We then run both StoVer1 and StoVer2 using the values $\{0.01, 0.04, 0.07, 0.10, 0.15\}$ for RSD and $\{0.01, 0.10, 0.15, 0.20\}$ for α.

The results for StoVer1 for $\alpha = 0.05$ are shown in Figure 20 where the resulting planned speed profiles are all very stable regardless of the RSD, although larger RSD values lead to lower desired speed. The same phenomenon can be observed for other values of α (not shown here). As for StoVer2, the results are shown in Figures 21 and 22 for $\alpha = 0.05$. In Figure 21, the planned speeds are reduced as RSD increases, and the speed profiles show a larger variability. The actual standard deviation of the speeds observed in the speed profile are shown in Table 9. The results suggest that a larger variability in the traffic speeds yields more fluctuations in the desired speed profiles, which is likely caused by the variability of the scenarios used in SAA while solving the StoVer2. This phenomenon is also observed in Figure 22, where larger values of RSD imply an increased variation in the traffic speeds. Similar observations are made for other values of α (not shown here). Generally speaking, planned speeds are significantly impacted by variability in traffic speeds, particularly for larger values of RSD, but not so much by α.

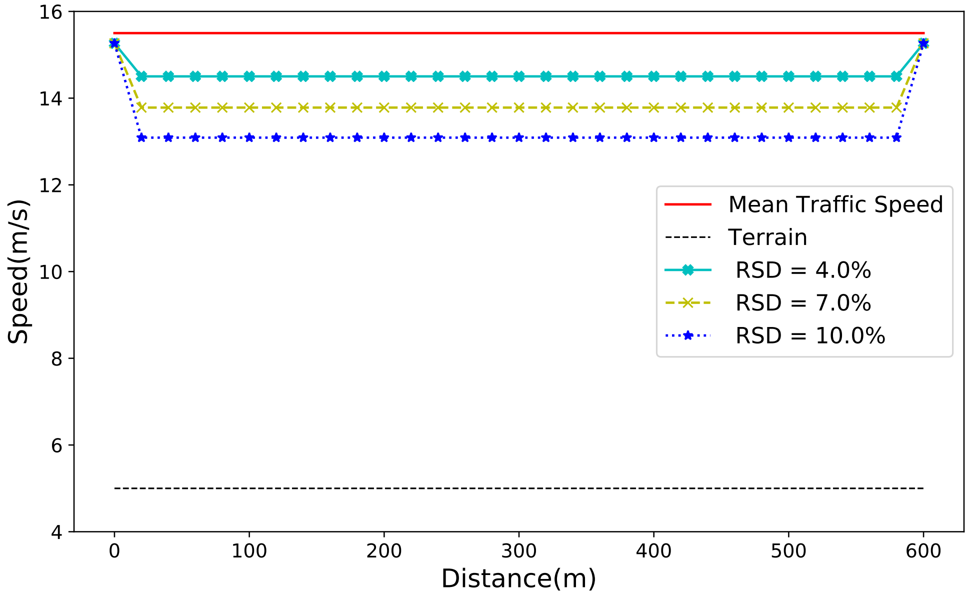

Figure 20: StoVer1 speed trajectories under varying RSDs ($\alpha = 0.05$)

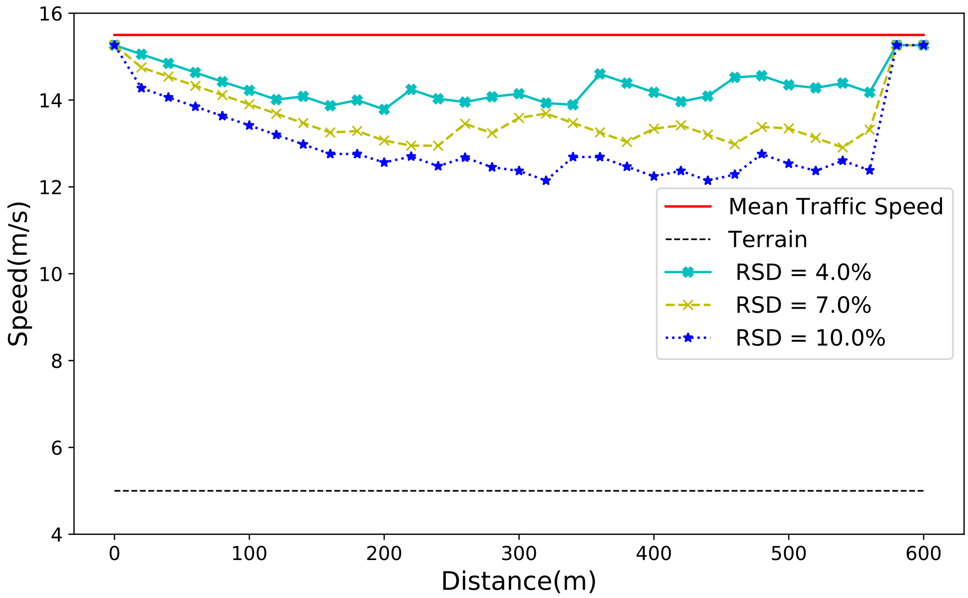

Figure 21: StoVer2 speed trajectories under varying RSDs ($\alpha = 0.05$)

Table 9: Standard deviations of StoVer2 speed profiles

	Relative standard deviation (RSD)				
α	0.01	0.04	0.07	0.10	0.15
0.02	0.05	0.33	0.61	0.72	0.91
0.05	0.02	0.36	0.57	0.73	0.93
0.10	0.03	0.33	0.63	0.73	0.89
0.15	0.03	0.28	0.52	0.74	0.97
0.20	0.03	0.31	0.52	0.77	0.94

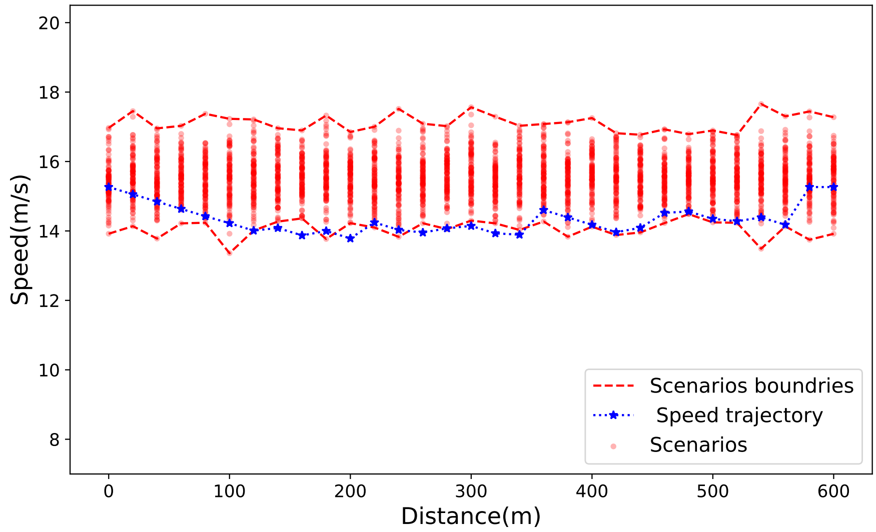

(a) RSD = 0.04

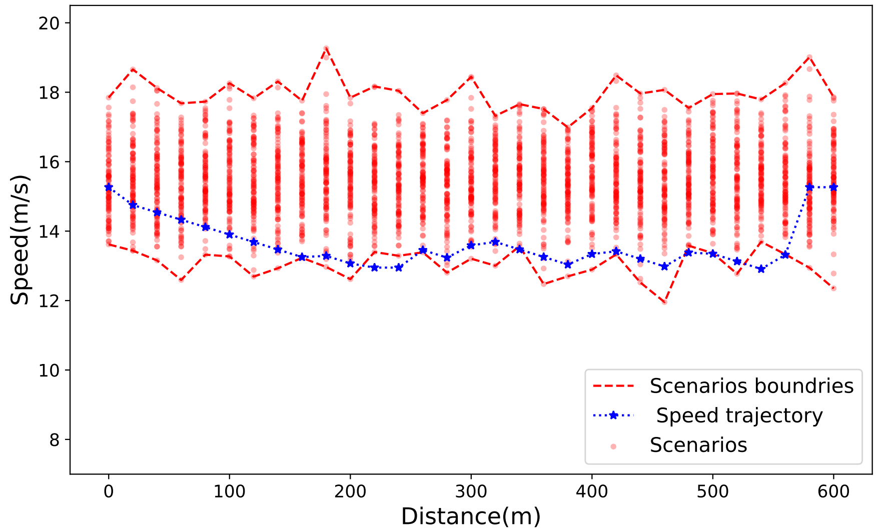

(b) RSD = 0.07

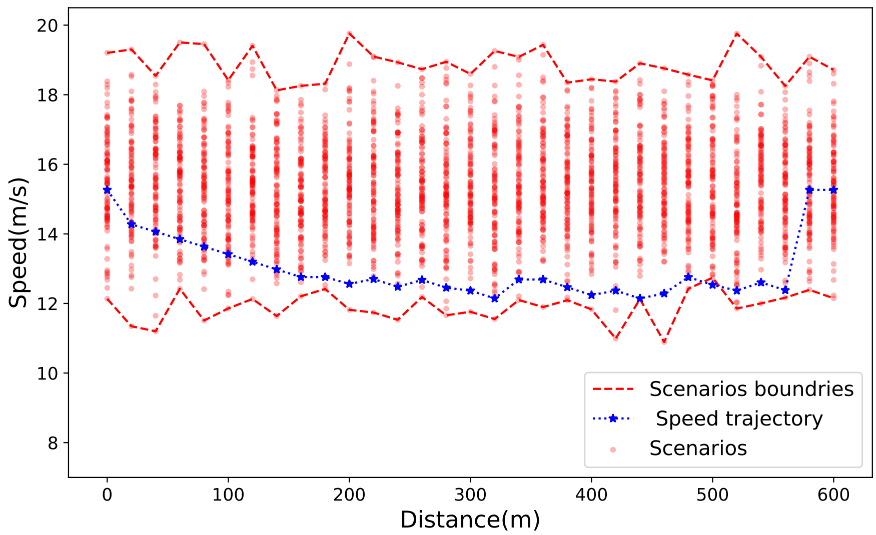

(c) RSD = 0.10

Figure 22: The scenarios used for different RSDs

6.4 The impact of the journey time limit

To assess the impact of varying the journey time limit, we solve StoVer1 and StoVer2 under 1000 scenarios using values $T \in \{60, 62.5, 65, 70, 75\}$ seconds. The results of StoVer1 under $\alpha = 0.05$ and $RSD = 0.1$ are shown in Figure 23 and in Tables 10 and 11. The results suggest that, as the journey duration increases, the time chance constraint is relaxed, which in turn reduces the desired speeds over several segments. The tables show reduced amounts of fuel consumed and a lower percentage of traffic speed violations as the trip duration increases. When the time period is long enough (70 s or longer), both fuel consumption and percentage of speed violations remain the same, indicating that the desired speed trajectories do not change.

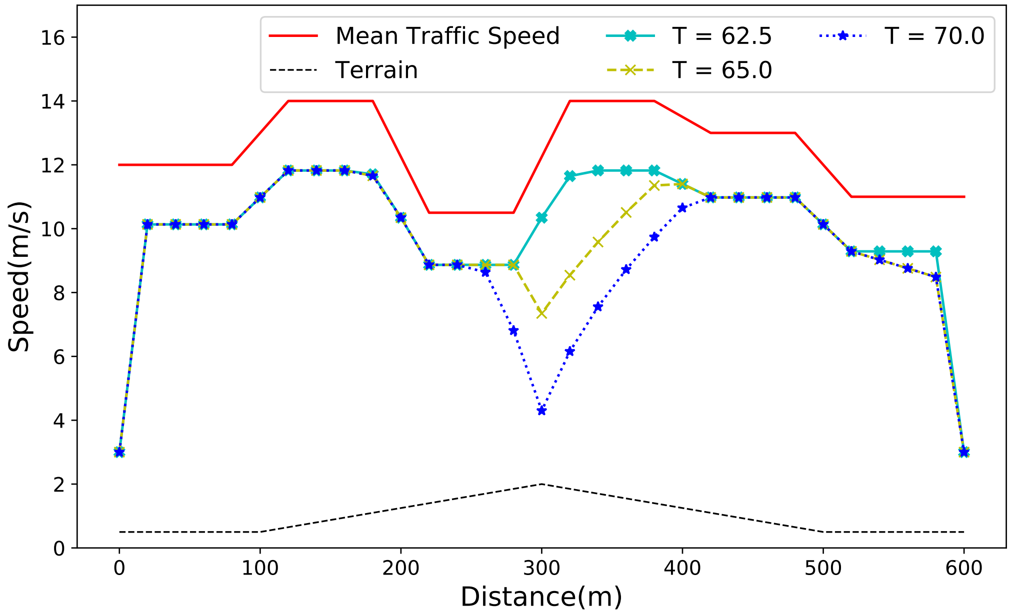

Figure 23: StoVer1 speed trajectories under different journey time limits

Table 10: Average fuel consumption (Gram) of StoVer1 speed profiles over 1000 scenarios ($\alpha = 0.05$)

	Time Period (T)				
α	60	62.5	65	70	75
0.02	NaN	NaN	129.92	117.93	117.54
0.05	NaN	134.17	120.27	116.78	116.79
0.10	NaN	122.19	117.92	116.64	116.64
0.15	128.88	120.03	117.57	117.01	117.01
0.20	125.10	119.66	117.96	117.69	117.69

Table 11: Percentage of speed violations over 1000 scenarios

	Time Period (T)				
α	60	62.5	65	70	75
0.02	NaN	NaN	1.83%	1.41%	1.36%
0.05	NaN	4.77%	3.65%	3.22%	3.18%
0.10	NaN	7.46%	6.83%	6.40%	6.40%
0.15	12.16%	10.44%	9.84%	9.26%	9.26%
0.20	14.75%	13.40%	12.66%	12.19%	12.19%

As for StoVer2, the results for $\alpha = 0.05$ are shown in Figure 24, and in Tables 12 and 13. Here, the result suggests that a looser trip time constraint leads to lower desired speed, but the speed trajectories themselves deviate over a larger part of the journey as compared to those in Figure 24. Tables 12 and 13 indicate similar findings as in StoVer1. In particular, as the time period is increased, the amount of fuel consumed and the probability of violating the time limit both decrease. When the time period is long enough (70s or more), the fuel consumption and probability of speed violation do not change, indicating that the desired speed trajectories are also unchanged.

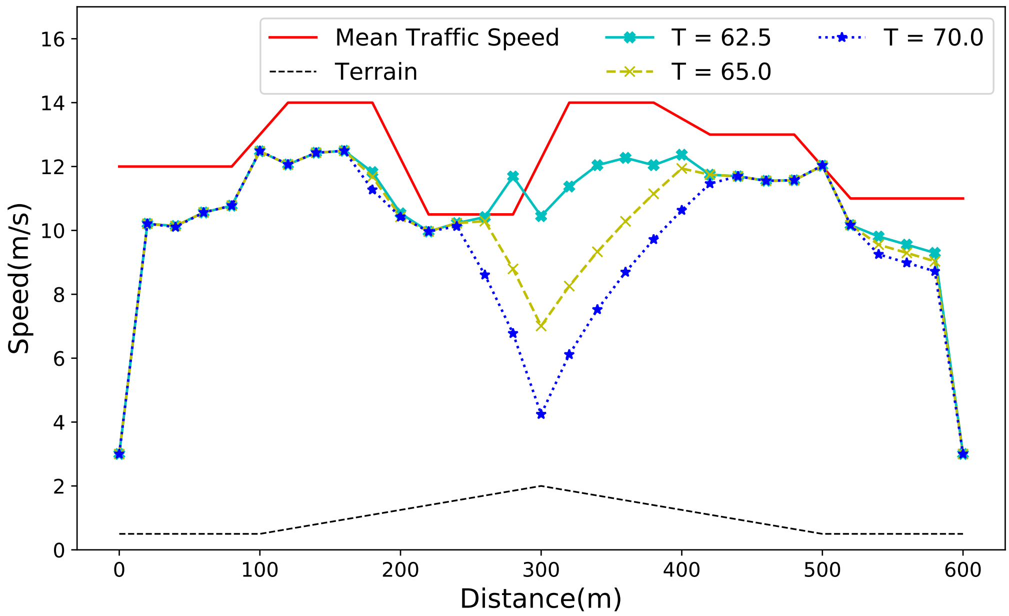

Figure 24: StoVer2 speed trajectories under different journey time limits ($\alpha = 0.05$)

Table 12: Average fuel consumption (Gram) of StoVer2 speed profiles over 1000 Scenarios

	Time Period (s)				
α	60	62.5	65	70	75
0.02	NaN	NaN	125.57	116.36	116.21
0.05	NaN	129.62	118.94	116.21	116.22
0.10	NaN	121.29	117.56	116.22	116.25
0.15	127.57	119.78	117.15	116.22	116.22
0.20	124.72	119.24	117.02	116.24	116.22

Table 13: Percentage of journey duration violations of StoVer2 speed profiles over 1000 scenarios

	Time Period (s)				
α	60	62.5	65	70	75
0.02	NaN	NaN	0	0	0
0.05	NaN	0	0	0	0
0.10	NaN	0.1%	0.2%	0	0
0.15	6.9%	11.7%	14.9%	0	0
0.20	39.1%	39.0%	38.1%	0	0

6.5 Performance of robust stochastic speed optimal control model

The final set of experiments are conducted to assess the performance of the model RStoVer1 presented in Section 5.1 tested using values $\eta \in \{0.01, 0.05, 0.10, 0.20\}$ representing different uncertainty sets. We use the same instance as in the Section 6.2 and set $T = 65$ seconds, $\alpha \in \{0.05, 0.10, 0.15, 0.20\}$ and $RSD = 0.07$. The nominal distribution P is assumed to be lognormal, with the mean values in Figure 3.

To simplify the calculations, for each η, we assume that the true distribution is a new lognormal distribution with the same mean as the nominal distribution but a larger RSD, and use it to generate 1000 test scenarios. We then calculate the fuel consumption and the percentage of speed violations for StoVer1 and RStoVer1, respectively. RStoVer1 increases the computational burden and leads to a more conservative solution when compared to StoVer1. The results are given in Table 14 and Figure 25.

According to Table 14, RStoVer1 is infeasible when $\eta = 0.20$ and $\alpha = 0.05$; in other cases, the fuel consumption output by StoVer1 and RStoVer1 increases as η increases. As for the frequency of the planned speeds exceeding the traffic speeds, the solutions obtained by StoVer1 violate the α value when $\eta = 0.10$ or larger, while those obtained by RStoVer1 are always below the α value. These results suggest that RStoVer1 avoids speed violation for large η (i.e., large uncertainty set), even for small values of α.

Comparing the results of different α, we find that as η increases, the uncertainty set is larger and thus $\bar{\alpha}$ is smaller, which reduces the desired speed in the most parts of the journey except on some segments due to the trip time constraint, as shown in Figure 25. Finally, for larger values of α, the speed trajectories are less impacted by η.

Table 14: The performance of robust StoVer1

			Fuel Consumption (Gram)		Percentage of Speed Violation	
α	η	$\bar{\alpha}$	Robust	StoVer1	Robust	StoVer1
0.05	0.01	0.025	117.41	116.40	2.61%	4.58%
0.05	0.05	0.008	120.19	116.79	1.98%	6.04%
0.05	0.10	0.003	125.27	117.11	1.50%	7.11%
0.05	0.20	0.000	NaN	117.73	NaN	8.82%
0.10	0.01	0.063	116.26	116.09	5.20%	7.51%
0.10	0.05	0.031	117.20	116.45	4.12%	9.10%
0.10	0.10	0.017	118.51	117.07	3.74%	10.72%
0.10	0.20	0.006	121.92	118.07	3.19%	12.31%
0.15	0.01	0.104	116.01	116.19	7.54%	9.89%
0.15	0.05	0.061	116.59	116.94	6.65%	11.96%
0.15	0.10	0.038	117.32	117.69	5.93%	13.15%
0.15	0.20	0.017	118.74	118.85	5.34%	15.03%
0.20	0.01	0.104	116.18	116.67	10.24%	13.05%
0.20	0.05	0.061	116.51	117.54	8.93%	14.53%
0.20	0.10	0.038	116.83	118.16	8.13%	16.18%
0.20	0.20	0.017	117.81	119.44	7.33%	17.49%

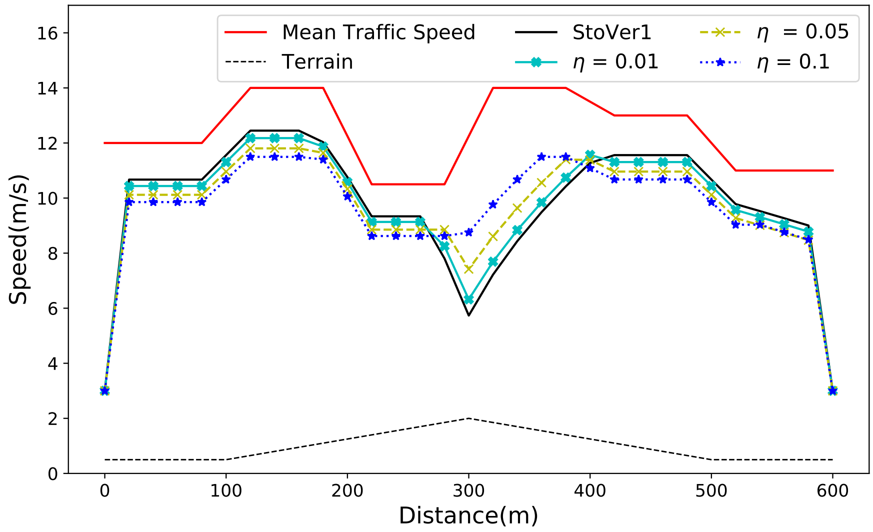

(a) $\alpha = 0.05$

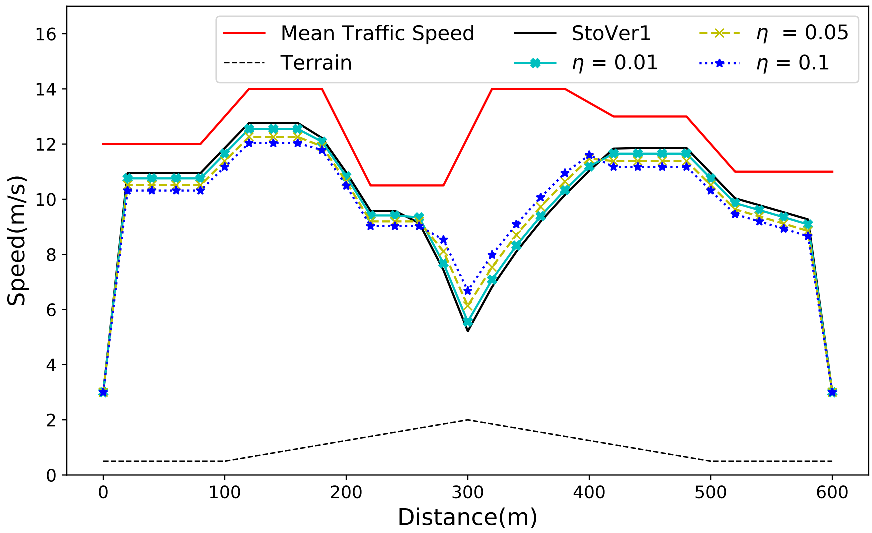

(b) $\alpha = 0.1$

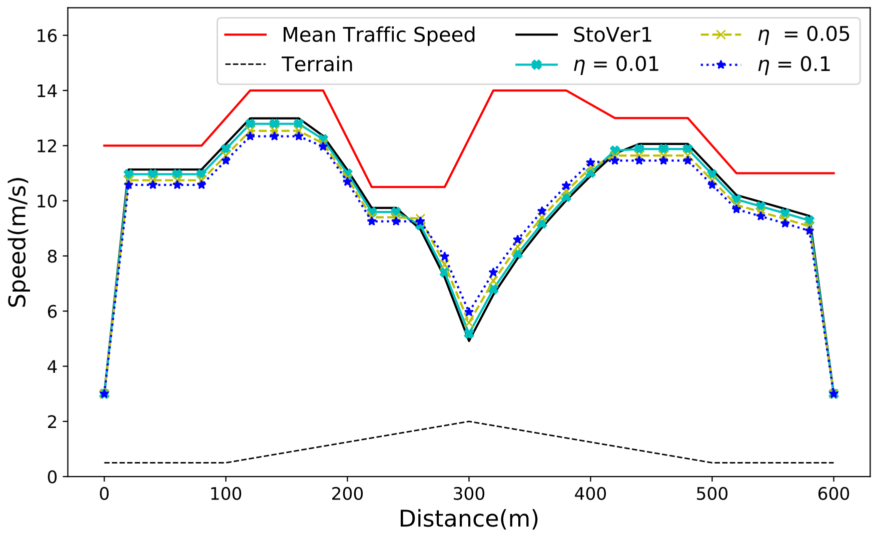

(c) $\alpha = 0.15$

Figure 25: Speed trajectories obtained by RStoVer1

7 Conclusions

In this paper, we proposed several ways to incorporate the uncertainties in surrounding traffic speeds into the optimal speed control problem. Specially, we described two stochastic optimal speed control models, one limiting the speed violations and the other trip durations. Based on these models, we further described their distributionally robust versions. To solve the proposed models, we proposed techniques to represent the models as nonlinear and mixed-integer programming formulations, using which we conducted numerical experiments to investigate the impact of the said uncertainties on the fuel economy and journey duration. The main findings are summarized as follows:

- Traffic speed uncertainty can significantly hinder the implementation of the planned speeds (given by the deterministic optimal control model) in a vehicle journey. This, in turn, increases the amount of fuel consumption and journey duration, but can be mitigated by incorporating the traffic speed uncertainty at the planning stage.
- The impact of traffic speed uncertainty is reduced as the time limit on the journey is increased.
- The planned speed profiles tend to exhibit lower speeds with larger traffic speed uncertainty sets, which ensures robustness against variability.

Extensions of our study may warrant further consideration for future research. First, as shown in the case studies, the computation time for StoVer2 is long, suggesting the need to improve the computational efficiency of the solution method. Second, where the traffic is oversaturated in parts of the journey, the traffic speed will be zero, which could lead to the infeasibility of our proposed methods as the journey time will be infinite. Incorporating oversaturation into the stochastic models would be another potential future research direction. Third, besides improving the models, we may integrate the stochastic optimal control with vehicle routing and scheduling, so as to further reduce the fuel consumption of a journey. Such an integration can be found in Liu et al. (2020) where the objective is to minimize the travel time and energy consumption of the vehicles without uncertainties in the traffic speed. Fourth, although our models are primarily intended for use in highways which do not usually have signalized intersections, they can be extended to account for uncertainties resulting from signals by using scenarios that represent the possible cases that arise as a vehicle approaches a signalized intersection (Bakibillah et al., 2019). Finally, the uncertainty in the vehicle system dynamics (i.e., perception errors of sensors) is likely to affect the implementation of planned speed profiles. Incorporating such uncertainty in the model would improve the applicability and performance of our proposed methods.

Acknowledgements

The authors gratefully acknowledge funding provided by the National Natural Science Foundation of China (No.71632008, 71501127). Thanks are due to the two anonymous reviewers whose detailed and valuable comments have helped to improve both the content and the exposition of the paper.

References

Akcelik, R. and Besley, M., 2003. Operating cost, fuel consumption, and emission models in aaSIDRA and aaMOTION. In 25th Conference of Australian Institutes of Transport Research, University of South Australia Adelaide, Australia, December, 2003.

Albrecht, A., Howlett, P., Pudney, P., Vu, X. and Zhou, P., 2016a. The key principles of optimal train control—Part 1: Formulation of the model, strategies of optimal type, evolutionary lines, location of optimal switching points. Transportation Research Part B: Methodological, 94, 482–508.

Albrecht, A., Howlett, P., Pudney, P., Vu, X. and Zhou, P., 2016b. The key principles of optimal train control—Part 2: Existence of an optimal strategy, the local energy minimization principle, uniqueness, computational techniques. Transportation Research Part B: Methodological, 94, 509–538.

Bakibillah, A.S.M., Kamal, M.A.S., Tan, C.P., Hayakawa, T. and Imura, J.I., 2019. Event-driven stochastic eco-driving strategy at signalized intersections from self-driving data. IEEE Transactions on Vehicular Technology, 68(9), 8557-8569.

Barth, M. and Boriboonsomsin, K., 2008. Real-world carbon dioxide impacts of traffic congestion. Transportation Research Record, 2058(1), 163–171.

Barth, M., Younglove, T. and Scora, G., 2005. Development of a heavy-duty diesel modal emissions and fuel consumption model. Tech. rep. UCB-ITS-PRR-2005-1, California PATH Program, Institute of Transportation Studies, University of California at Berkeley.

Bektaş, T., Ehmke, J.F., Psaraftis, H.N. and Puchinger, J., 2019. The role of operational research in green freight transportation. European Journal of Operational Research, 274(3), 807–823.

Bektaş, T. and Laporte, G., 2011. The pollution-routing problem. Transportation Research Part B: Methodological, 45(8), 1232–1250.

Bender, F.A., Kaszynski, M. and Sawodny, O., 2013. Drive cycle prediction and energy management optimization for hybrid hydraulic vehicles. IEEE Transactions on vehicular technology, 62(8), 3581–3592.

Ben-Tal, A., El Ghaoui, L. and Nemirovski, A., 2009. Robust optimization (Vol. 28). Princeton, New Jersey, America: Princeton University Press.

Bertsekas, D.P., 1995. Dynamic programming and optimal control Vols. 1 and 2. Belmont, MA: Athena Scientific.

Chang, D.J. and Morlok, E.K., 2005. Vehicle speed profiles to minimize work and fuel consumption. Journal of Transportation Engineering, 131(3), 173–182.

Chen, W., Sim, M., Sun, J. and Teo, C.P., 2010. From CVaR to uncertainty set: Implications in joint chance-constrained optimization. Operations Research, 58, 470-485.

Claussmann, L., Revilloud, M., Gruyer, D. and Glaser, S., 2019. A review of motion planning for highway autonomous driving. IEEE Transactions on Intelligent Transportation Systems, 21(5), 1826–1848.

De Nunzio, G., De Wit, C.C., Moulin, P. and Di Domenico, D., 2016. Eco-driving in urban traffic networks using traffic signals information. International Journal of Robust and Nonlinear Control, 26(6), 1307–1324.

Demir, E., Bektaş, T. and Laporte, G., 2014. The bi-objective pollution-routing problem. European Journal of Operational Research, 232(3), 464–478.

Dib, W., Chasse, A., Moulin, P., Sciarretta, A. and Corde, G., 2014. Optimal energy management for an electric vehicle in eco-driving applications. Control Engineering Practice, 29, 299–307.

Franke, R., Terwiesch, P., Meyer, M., 2000. An algorithm for the optimal control of the driving of trains. In: Proceedings of the 39th IEEE Conference on Decision and Control, Sydney, Australia, 2000, pp. 2123–2128.

Fröberg, A., Hellström, E. and Nielsen, L., 2006. Explicit fuel optimal speed profiles for heavy trucks on a set of topographic road profiles. SAE Technical Paper.

Gong, S. and Du, L., 2018. Cooperative platoon control for a mixed traffic flow including human drive vehicles and connected and autonomous vehicles. Transportation Research Part B: Methodological, 116, 25–61.

Guo, L., Gao, B., Gao, Y. and Chen, H., 2016. Optimal energy management for HEVs in eco-driving applications using bi-level MPC. IEEE Transactions on Intelligent Transportation Systems, 18(8), 2153–2162.

Han, J., Sciarretta, A., Ojeda, L.L., De Nunzio, G. and Thibault, L., 2018. Safe-and eco-driving control for connected and automated electric vehicles using analytical state-constrained optimal solution. IEEE Transactions on Intelligent Vehicles, 3(2), 163–172.

Hellström, E., Åslund, J. and Nielsen, L., 2010. Design of an efficient algorithm for fuel-optimal look-ahead control. Control Engineering Practice, 18(11), 1318–1327.

Hellström, E., Fröberg, A. and Nielsen, L., 2006. A real-time fuel-optimal cruise controller for heavy trucks using road topography information. SAE Technical Paper.

Hellström, E., Ivarsson, M., Åslund, J. and Nielsen, L., 2009. Look-ahead control for heavy trucks to minimize trip time and fuel consumption. Control Engineering Practice, 17(2), 245–254.

Heppeler, G., Sonntag, M. and Sawodny, O., 2014. Fuel efficiency analysis for simultaneous optimization of the velocity trajectory and the energy management in hybrid electric vehicles. IFAC Proceedings Volumes, 47(3), 6612–6617.

Hofleitner, A., Herring, R. and Bayen, A., 2012. Probability distributions of travel times on arterial networks: a traffic flow and horizontal queuing theory approach. In 91st Transportation Research Board Annual Meeting , Washington D.C, America, 22-26 January, 2012.

Hooker, J.N., 1988. Optimal driving for single-vehicle fuel economy. Transportation Research Part A: Policy and Practice, 22(3), 183–201.

Hooker, J.N., Rose, A.B. and Roberts, G.F., 1983. Optimal control of automobiles for fuel economy. Transportation Science, 17(2), 146–167.

Hu, Z. and Hong, L.J., 2013. Kullback-Leibler divergence constrained distributionally robust optimization. Available at Optimization Online.

Katrakazas, C., Quddus, M., Chen, W.H. and Deka, L., 2015. Real-time motion planning methods for autonomous on-road driving: State-of-the-art and future research directions. Transportation Research Part C: Emerging Technologies, 60, 416–442.

Kim, T.S., Manzie, C. and Sharma, R., 2009. Model predictive control of velocity and torque split in a parallel hybrid vehicle. In 2009 IEEE International Conference on Systems, Man and Cybernetics, San Antonio, Texas, America, October, 2009.

Kopp, R.E., 1962. Pontryagin maximum principle. In Mathematics in Science and Engineering, Vol. 5, 255–279.

Leong, H.J., 1968. The distribution and trend of free speeds on two lane two way rural highways in New South Wales. In Australian Road Research Board (ARRB) Conference, 4th, 1968, Melbourne (Vol. 4, No. 1).

Lim, H., Su, W. and Mi, C.C., 2016. Distance-based ecological driving scheme using a two-stage hierarchy for long-term optimization and short-term adaptation. IEEE Transactions on Vehicular Technology, 66(3), 1940–1949.

Liu, T., Azarm, S. and Chopra, N., 2020. Integrating Optimal Vehicle Routing and Control With Load-Dependent Vehicle Dynamics Using a Confidence Bounds for Trees-Based Approach. Journal of Dynamic Systems, Measurement, and Control, 142(4).

Luján, J.M., Guardiola, C., Pla, B. and Reig, A., 2018. Fuel and pollutant efficient vehicle speed optimization in real driving conditions. IFAC-PapersOnLine, 51(31), 225–232.

Ma, J., Li, X., Zhou, F., Hu, J. and Park, B.B., 2017. Parsimonious shooting heuristic for trajectory design of connected automated traffic part II: Computational issues and optimization. Transportation Research Part B: Methodological, 95, 421–441.

Maamria, D., Gillet, K., Colin, G., Chamaillard, Y. and Nouillant, C., 2016a. Which methodology is more appropriate to solve eco-driving optimal control problem for conventional vehicles? In 2016 IEEE Conference on Control Applications (CCA), Buenos Aires, Argentina, September, 2016.

Maamria, D., Gillet, K., Colin, G., Chamaillard, Y. and Nouillant, C., 2016b. On the use of Dynamic Programming in eco-driving cycle computation for electric vehicles. In 2016 IEEE Conference on Control Applications (CCA), Buenos Aires, Argentina, September, 2016.

Mensing, F., Trigui, R. and Bideaux, E., 2012. Vehicle trajectory optimization for hybrid vehicles taking into account battery state-of-charge. In 2012 IEEE vehicle Power and Propulsion Conference, Seoul, Korea, 9-12 October, 2012.

Monastyrsky, V.V. and Golownykh, I.M., 1993. Rapid computation of optimal control for vehicles. Transportation Research Part B: Methodological, 27(3), 219–227.

Nasri, M.I., Bektaş, T. and Laporte, G., 2018. Route and speed optimization for autonomous trucks. Computers & Operations Research, 100, 89–101.

Nemirovski, A. and Shapiro, A., 2007. Convex approximations of chance constrained programs. SIAM Journal on Optimization, 17(4), 969–996.

Ojeda, L.L., Han, J., Sciarretta, A., De Nunzio, G. and Thibault, L., 2017. A real-time eco-driving strategy for automated electric vehicles. In 2017 IEEE 56th Annual Conference on Decision and Control (CDC), Melbourne, Australia, 12-15 December, 2017.

Ozatay, E., Ozguner, U., Michelini, J. and Filev, D., 2014. Analytical solution to the minimum energy consumption based velocity profile optimization problem with variable road grade. IFAC Proceedings Volumes, 47(3), 7541–7546.

Park, B.J., Zhang, Y. and Lord, D., 2010. Bayesian mixture modeling approach to account for heterogeneity in speed data. Transportation Research Part B: Methodological, 44(5).662-673.

Passenberg, B., Kock, P. and Stursberg, O., 2009. Combined time and fuel optimal driving of trucks based on a hybrid model. In 2009 European Control Conference, Budapest, Hungary, 23-26 August, 2009.

Petit, N. and Sciarretta, A., 2011. Optimal drive of electric vehicles using an inversion-based trajectory generation approach. IFAC Proceedings Volumes, 44(1), 14519–14526.

Pisu, P. and Rizzoni, G., 2007. A comparative study of supervisory control strategies for hybrid electric vehicles. IEEE transactions on control systems technology, 15(3), 506–518.

Rakha, H.A., El-Shawarby, I., Arafeh, M. and Dion, F., 2006. Estimating path travel-time reliability. In 2006 IEEE Intelligent Transportation Systems Conference, Baltimore, Maryland, America, September, 2006, pp. 236–241.

Schwarzkopf, A.B. and Leipnik, R.B., 1977. Control of highway vehicles for minimum fuel consumption over varying terrain. Transportation Research, 11(4), 279–286.

Sciarretta, A. and Guzzella, L., 2007. Control of hybrid electric vehicles. IEEE Control Systems Magazine, 27(2), 60–70.

Scora, G. and Barth, M., 2006. Comprehensive modal emissions model (cmem), version 3.01. User guide. Centre for environmental research and technology. University of California, Riverside, 1070.

Shapiro, A., Dentcheva, D. and Ruszczyński, A., 2009. Lectures on stochastic programming: modeling and theory. Philadelphia: Society for Industrial and Applied Mathematics.

van Keulen, T., de Jager, B., Foster, D. and Steinbuch, M., 2010. Velocity trajectory optimization in hybrid electric trucks. In Proceedings of the 2010 American Control Conference, Marriott Waterfront, Baltimore, America, June, 2010 pp. 5074–5079.

Wang, Y., De Schutter, B., Ning, B., Groot, N. and Van Den Boom, T.J., 2011. Optimal trajectory planning for trains using mixed integer linear programming. In 2011 14th International IEEE Conference on Intelligent Transportation Systems (ITSC), Washington, America, October, 2011.

Wang, Y., De Schutter, B., van den Boom, T.J. and Ning, B., 2013. Optimal trajectory planning for trains–A pseudospectral method and a mixed integer linear programming approach. Transportation Research Part C: Emerging Technologies, 29.97–114.

Wei, J., Dolan, J.M., Snider, J.M. and Litkouhi, B., 2011. A point-based mdp for robust single-lane autonomous driving behavior under uncertainties. In 2011 IEEE International Conference on Robotics and Automation, Shanghai, China, 9-13 May, 2011.

Wu, X., He, X., Yu, G., Harmandayan, A. and Wang, Y., 2015. Energy-optimal speed control for electric vehicles on signalized arterials. IEEE Transactions on Intelligent Transportation Systems, 16(5), 2786–2796.

Xu, G., Li, W., Xu, K. and Song, Z., 2011. An intelligent regenerative braking strategy for electric vehicles. Energies, 4(9), 1461–1477.

Yang, H., Rakha, H. and Ala, M.V., 2016. Eco-cooperative adaptive cruise control at signalized intersections considering queue effects. IEEE Transactions on Intelligent Transportation Systems, 18(6), 1575–1585.

Ye, H. and Liu, R., 2016. A multiphase optimal control method for multi-train control and scheduling on railway lines. Transportation Research Part B: Methodological, 93, 377–393.

Ye, H. and Liu, R., 2017. Nonlinear programming methods based on closed-form expressions for optimal train control. Transportation Research Part C: Emerging Technologies, 82, 102–123.

Zhao, W., Ngoduy, D., Shepherd, S., Liu, R. and Papageorgiou, M., 2018. A platoon based cooperative eco-driving model for mixed automated and human-driven vehicles at a signalised intersection. Transportation Research Part C: Emerging Technologies, 95, 802–821.

Zhou, F., Li, X. and Ma, J., 2017. Parsimonious shooting heuristic for trajectory design of connected automated traffic part I: Theoretical analysis with generalized time geography. Transportation Research Part B: Methodological, 95, 394–420.

Zou, Y. and Zhang, Y., 2011. Use of skew-normal and skew-t distributions for mixture modeling of freeway speed data. Transportation Research Record, 2260(1), 67-75.

Appendix A. Introduction to the comprehensive modal emissions model

In this part, we briefly introduce the comprehensive modal emissions model (CMEM) described by Barth et al. (2005), Scora and Barth (2006), and Barth and Boriboonsomsin (2008), which is an instantaneous model estimating fuel consumption rate of heavy-goods vehicles. The core of the model is the total tractive power requirement P_{tract} (kilowatt) placed at the wheels, expressed as follows,

$$P_{tract} = (M\tau + 1/2 C_d \rho A v^2 + MgC_r \cos\theta + Mg\sin\theta)v/1000, \tag{A.1}$$

where M is the total vehicle weight (kilogram), τ is the acceleration (meter/second^2), C_d and C_r are the coefficients of the aerodynamic drag and rolling resistance, respectively, ρ is the air density (kilogram/meter^3), A is the frontal surface area of the vehicle (meter^2), v is the vehicle speed (meter/second), θ is the road angle (degree), and g is the gravitational constant (meter/second^2).

To avoid the total tractive power requirement (A.1) being negative under deceleration and road slope, the emissions framework described in Akcelik and Besley (2003) is further used, which leads to:

$$P_{tract} = \max\left\{(Ma + \frac{1}{2}C_d \rho A v^2 + MgC_r \cos\theta + Mg\sin\theta)v/1000, 0\right\}, \tag{A.2}$$

where a represents the rate of change in the speed, which is positive for acceleration and negative for deceleration.

Using P_{tract}, the fuel consumption rate FR (gram/second) is given by

$$FR = (\varkappa Q\Lambda + \frac{P_{tract}}{\gamma_{tf}\gamma} + \frac{P_{acc}}{\gamma})\frac{\zeta}{\kappa}, \tag{A.3}$$

where γ_{tf} is the vehicle drivetrain efficiency, P_{acc} (kilowatt) is the constant engine power demand associated with running losses of the engine and the operation of vehicle accessories, ζ is the fuel-to-air mass ratio, $\varkappa$ is the engine friction factor (kilojoule/revolution/liter), Q is the engine speed (revolution/second), Λ is the engine displacement (Liter), γ is the efficiency parameter for diesel engines, and κ is the heating value of a typical diesel fuel (kilojoule/gram).

Integrating the functions (A.2)–(A.3) above yields:

$$FR(v, a) = C_1 + C_2 \max\left\{Ma + \frac{1}{2}C_d \rho A v^2 + Mg\sin\theta + MgC_r \cos\theta, 0\right\} v, \tag{A.4}$$

where $C_1 = \zeta \varkappa Q \Lambda / \kappa + P_{acc} \zeta / \kappa \gamma$ and $C_2 = \zeta / 1000 \kappa \gamma \gamma_{tf}$.

Typical values of the model parameters used in this case study are from Demir et al. (2014) and shown in Table A.1.

Table A.1: Parameters used in the computational tests

Notation	Description	Typical values
w	Curb-weight(kilogram)	6350
ζ	Fuel-to-air mass ratio	1
$\varkappa$	Engine friction factor(kilojoule/revolution/liter)	0.2
Q	Engine speed(revolution/second)	33
Λ	Engine displacement (liter)	5
g	Gravitational constant (meter/second^2)	9.81
C_d	Coefficient of aerodynamic drag	0.7
ρ	Air density (kilogram/meter^2)	1.2041
A	Frontal surface area (meter^2)	3.912
C_r	Coefficient of rolling resistance	0.01
γ_{tf}	Vehicle drive train efficiency	0.4
γ	Efficiency parameter for diesel engines	0.9
κ	Heating value of a typical diesel fuel (kilojoule/gram)	44

Appendix B. Dynamic programming for deterministic optimal control model

For the dynamic programming (DP) used to solve the deterministic optimal control model (3.1)–(3.6), we use the method provided by Monastyrsky and Golownykh (1993). First, we modify the objective function (3.1) to the following function,

$$\mathbb{J} = \int_0^S FR(v(s), a(s)) \frac{1}{v(s)} \mathrm{d}s + \beta \int_0^S \frac{1}{v(s)} \mathrm{d}s, \tag{A.1}$$

where β is a constant and can be tuned to satisfy the journey time constraint (3.2) (Maamria et al., 2016a) .

We discretize the road as in Section 3.2.1, and then use the forward DP to solve the problem. Let the segment indices $0, 1, ..., n-1$ be the stages, $\mathbb{J}_k(v(k))$ be the minimum value of objective function (A.1) from stages 0 to k, given that the vehicle's speed is $v(k)$ at stage k. Then the optimal control for each stage is calculated by the recursive formula,

$$\mathbb{J}_{k+1}(v(k+1)) = \underset{a(k)}{\text{Minimize}} \left\{ FR(v(k), a(k)) \frac{\Delta s}{v(k)} + \mathbb{J}_k(v(k)) \right\}, \tag{A.2}$$

where $a(k) = \frac{v(k+1)^2 - v(k)^2}{2\Delta s}$, $a_{\min} \leq a(k) \leq a_{\max}$ and $\epsilon \leq v(k+1) \leq v_{\max}(k+1)$. The boundary condition is given as $v(0) = v_0, v(n) = v_S$.

It is worth mentioning that the value of β should be calculated by search, so the calculation time is the combination of searching β and DP. The algorithm we use for the numerical study is explained below,

Algorithm 2: Calculation of speed trajectory.

Initialization: Set $\beta = 0$

Step j**:** Set $\beta = \beta + \Delta\beta$

- Dynamic programming
- If journey time $\sum_{k=0}^{k=n-1} \frac{\Delta s}{v(k)} \geq T$, set $j = j + 1$.
- If journey time $\sum_{k=0}^{k=n-1} \frac{\Delta s}{v(k)} \leq T$, stop and return $\{v(0), v(1), ..., v(n-1), v(n)\}$.

where $\Delta\beta$ is a constant value.

For the case study in Section 6.1, we discretize the whole journey to 30 segments, which is same as other solution methods, and thus the number of stages is also 30. As for the solution algorithm for DP, we use the label correcting method (Bertsekas, 1995), where the speed is discretized by $0.1m/s$. Then we set $\Delta\beta = 0.02$ for Algorithm 2.

Appendix C. The impact of the traffic speed correlation

The uncertain traffic speeds may be spatially dependent with each other. Therefore, in this appendix, we investigate the applicability of our proposed stochastic models in the case of correlated traffic speeds.

We use multi-lognormal distribution with the same mean and standard deviation as Section 6.2.1, but with three different correlation matrices, which we refer to as low, moderately and highly correlated matrix, respectively. Table A.2 shows the low correlated matrix, where the indices indicate the road segments. The correlation between the adjacent segments is set to be the biggest, and the correlation decreases with the increasing distance between segments; the value of correlation is set to be from 0 to 0.30. The ranges of the correlation values in the moderately correlated matrix and highly correlated matrix range from 0 to 0.60 and from 0 to 0.90, respectively.

Table A.2: The correlation matrix of low correlated traffic speeds

Index	1	2	3	4	5	6	7	8	...	30
1	1.00	0.30	0.25	0.20	0.15	0.10	0.05	0	...	0
2	0.30	1.00	0.30	0.25	0.20	0.15	0.10	0.05	...	0
3	0.25	0.30	1.00	0.30	0.25	0.20	0.15	0.10	...	0
4	0.20	0.25	0.30	1.00	0.30	0.25	0.20	0.15	...	0
⋮	⋮	⋮	⋮	⋮	⋮	⋮	⋮	⋮	⋮	⋮
30	0	0	0	0	0	0	0	0	...	1.00

The chance constraint of StoVer1 is based on the marginal distribution, so the planned speed profiles are not impacted by the correlation. Fig A.1 shows the speed trajectories obtained by StoVer2 under different correlation matrixes. The difference between the speed profiles is caused by the scenarios generated under different correlation matrixes.

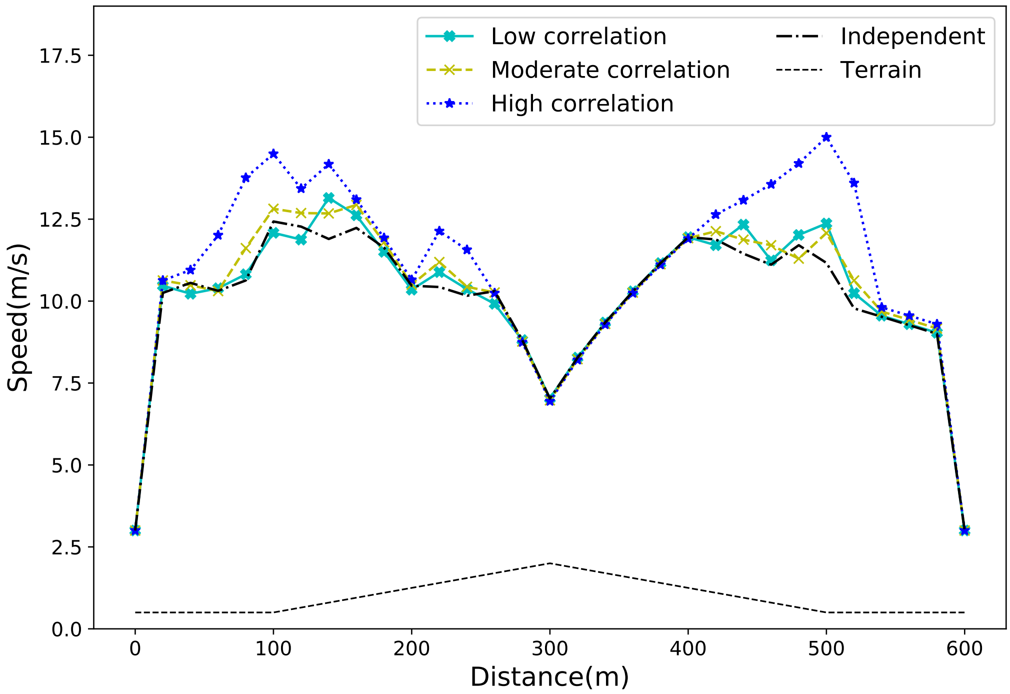

Figure A.1: Speed trajectories obtained by StoVer2 under different correlations ($\alpha = 0.05$)

To evaluate the performance of our proposed stochastic models under different correlated traffic speeds, the obtained speed profiles are evaluated in the same way as in Section 6.2.1. Table A.3 shows the statistics.

According to Table A.3, the fuel consumption of all models decreases with higher correlation, because the scenarios generated with higher correlation become more concentrated.

We can also see that the fuel consumption of the deterministic model is the most sensitive to the correlation.

For the speed violation (Table A.4), StoVer1 can guarantee that the percentage of speed violation satisfies the requirement under all correlation matrixes, while the deterministic model and StoVer2 cannot. Similar phenomena can be observed on the journey time duration (Table A.5).

Table A.3: Average fuel consumption (Gram) over 1000 correlated scenarios

	Low correlated			Moderately correlated			Highly correlated		
α	Deter	StoVer1	StoVer2	Deter	StoVer1	StoVer2	Deter	StoVer1	StoVer2
0.02	123.55	129.89	125.47	120.81	129.88	124.87	117.07	129.86	123.74
0.05	123.55	120.20	118.87	120.81	120.14	118.42	117.07	120.06	117.41
0.10	123.55	117.76	117.51	120.81	117.50	116.81	117.07	117.27	115.96

Table A.4: Percentage of speed violations over 1000 correlated scenarios

	Low correlated			Moderately correlated			Highly correlated		
α	Deter	StoVer1	StoVer2	Deter	StoVer1	StoVer2	Deter	StoVer1	StoVer2
0.02	29.66%	1.67%	18.33%	30.49%	1.58%	20.88%	29.73%	1.59%	41.94%
0.05	29.66%	3.42%	14.60%	30.49%	3.49%	18.22%	29.73%	4.01%	35.30%
0.10	29.66%	6.54%	15.17%	30.49%	6.36%	16.55%	29.73%	6.90%	32.58%

Table A.5: Percentage of journey time violations over 1000 correlated scenarios

	Low correlated			Moderately correlated			Highly correlated		
α	Deter	StoVer1	StoVer2	Deter	StoVer1	StoVer2	Deter	StoVer1	StoVer2
0.02	43.60%	27.10%	0	45.10%	20.80%	0	38.40%	12.80%	0
0.05	43.60%	48.80%	0	45.10%	35.70%	0.40%	38.40%	23.20%	1.40%
0.10	43.60%	72.60%	0.80%	45.10%	54.90%	3.60%	38.40%	35.60%	5.80%